Nanoscale Horizons

ROYAL SOCIETY OF CHEMISTRY

MINIREVIEW

View Article Online
View Journal | View Issue

Cite this: *Nanoscale Horiz.*, 2026, **11**, 114

Self-assembled DNA nanodevices for intelligent biosensing

Yongjian Chen,†[ab] Run Tian,†[ab] Yi Zhang,[c] Baoquan Ding *[ab] and Qiao Jiang *[ab]

Received 29th June 2025,
Accepted 3rd October 2025

DOI: 10.1039/d5nh00446b

rsc.li/nanoscale-horizons

Leveraging sequence specificity, shape programmability, and spatial addressability, DNA nanotechnology enables the nanometer-precise construction of DNA nanodevices for a wide range of biological applications. This minireview summarizes recent progress in employing self-assembled DNA nanostructures as scaffolds for creating advanced nanodevices as biosensors. We highlight notable advancements in ultrasensitive detection, multiplexed sensing, and targeted molecular bioimaging. These self-assembled DNA nanodevices are designed for intelligent sensing of various analytes, offering innovative solutions for biomedical diagnostics and environmental surveillance. Challenges related to the detection precision, stability, and scalable production of these promising DNA-based biosensors are also discussed.

1. Introduction

Deoxyribonucleic acid (DNA) is notable for its fundamental role as the primary carrier of genetic information in almost all living organisms.[1,2] Beyond its biological function, DNA has emerged as a versatile and programmable material for nanoscale engineering, giving rise to the vibrant field of DNA nanotechnology. In the early 1980s, Nadrian Seeman conceived the idea of using DNA molecules as building blocks to create artificial DNA assemblies.[3] His group demonstrated the feasibility of constructing stable, synthetic, branched DNA junctions with sticky ends that could self-assemble into predetermined patterns. This finding inspired the development of tile-based DNA structures, including multi-arm structures, two-dimensional (2D) arrays, polyhedral structures and three-dimensional (3D) crystals.[4–8] Another major milestone came in 2006 with Paul Rothemund's invention of DNA origami.[9] The fabrication of DNA origami involves folding a bacteriophage-derived single-stranded scaffold strand over 7000 bases into an arbitrary shape using hundreds of shorter staple strands. This method

[a] *CAS Key Laboratory of Nanosystem and Hierarchical Fabrication, CAS Center for Excellence in Nanoscience, National Center for Nanoscience and Technology, Beijing 100190, China. E-mail: dingbq@nanoctr.cn, jiangq@nanoctr.cn*
[b] *University of Chinese Academy of Sciences, Beijing 100049, China*
[c] *Department of Physiology and Medical Biology, Medical College, Dalian University, Dalian 116600, China*
† These authors contributed equally to this work.

Yongjian Chen

Yongjian Chen graduated from the University of Chinese Academy of Sciences (UCAS) with a bachelor's degree in chemistry in 2021. He then received his master's degree in physical chemistry from the National Center for Nanoscience and Technology (NCNST) in 2024. He is now a PhD candidate at NCNST under the supervision of Professors Baoquan Ding and Qiao Jiang. His research focuses on design of functional DNA nanostructures and their biomedical applications.

Run Tian

Dr. Run Tian obtained his bachelor's degree in Pharmaceutical Engineering from Jilin University in 2018. He then gained his master's degree from the National Center for Nanoscience and Technology (NCNST), and PhD degree from Sino-Danish College, University of Chinese Academy of Sciences. He is now a post-doctoral research fellow in NCNST. His research interests focus on design of functional DNA nanostructures and their biomedical applications.

enables the creation of a wide variety of 2D and 3D DNA structures with diverse morphologies and even dynamic structures.[10–19]

DNA nanotechnology has paved the way for a wide range of self-assembled DNA nanodevices with tangible applications by harnessing the sequence specificity, shape programmability, and spatial addressability of DNA nanostructures. In particular, self-assembled DNA biosensors have emerged as innovative tools for a variety of chemical and biological applications, including disease diagnosis, pathogen detection, and environmental monitoring. Serving as programmable and addressable templates, DNA nanostructures facilitate the spatial assembly and organization of multiple functional payloads, including small molecular dyes, peptides, proteins, nucleic acids, nanoparticles, *etc.*, with nanoscale precision.[20–26] This assembling capability allows DNA nanotechnology for the creation of nanodevices with tailored properties for smart sensing tasks. Significant advancements have been made in the design of dynamic DNA-based devices and machines, which are essential for building DNA-based sensing devices. For instance, strand displacement has been exploited in constructing DNA walkers as molecular processors.[27] Reciprocating DNA nanomachines with flexible structures enable the fabrication of DNA motors and nanorobots.[28–30] Stimuli-responsive dynamic DNA nanodevices capable of undergoing fine-tuned structural reconfiguration can also be fabricated, releasing the payloads upon receiving the desired signals.[31–36] Furthermore, the inherent biocompatibility of DNA nanodevices has been exploited to engineer smart sensing systems.

In this minireview, we will explore the function of DNA nanodevices in the field of biosensing. Notable advancements in ultrasensitive detection, multiplexed sensing, and targeted molecular bioimaging are also summarized. The discussion covers possible challenges for these novel nanoprobes, including concerns about detection precision, capabilities, pharmacokinetic properties, stability, immunogenicity, and scalable mass production.

2. Design of self-assembled DNA nanodevices for biosensing

To perform specific biosensing tasks, a typical DNA nanodevice-based biosensor is designed by incorporating sensing and reporting elements onto self-assembled DNA scaffolds (Fig. 1). Sensing elements are responsible for recognizing and binding to target molecules. Engineered DNA sensors utilize various functional nucleic acids, including G-quadruplexes, i-motifs, aptamers, and DNAzymes,[37–41] that can conveniently be integrated into DNA scaffolds, as probing components to enable sensitive recognition of target analytes. The sensing capabilities can be further broadened by conjugating DNA scaffolds with small-molecule ligands, peptides, and antibodies for specific molecular targets.[42–44] Moreover, multiple

Yi Zhang

Yi Zhang obtained a bachelor's degree in Biological Engineering from Dalian Polytechnic University in 2022. He is currently a master's student in a joint program between the School of Medicine at Dalian University and the National Center for Nanoscience and Technology. His research is supervised by Professors Mingfei Lang, Baoquan Ding, and Qiao Jiang. His research focuses on the functionalization of cells with nanoscale DNA and its applications in cancer treatment.

Baoquan Ding

Professor Baoquan Ding received his BS in Chemistry from Jilin University in 2000. He obtained his PhD in 2006 from the Department of Chemistry at New York University, under the supervision of Professor Nadrian Seeman. He completed his postdoctoral work at the Molecular Foundry, Lawrence Berkeley National Laboratory. He joined the Biodesign Institute, Arizona State University, as a research assistant professor in October 2009. He established his research group as a professor in National Center for Nanoscience and Technology, China, in November 2010. His research interests include DNA nanotechnology, co-assembled biomolecules and drug delivery.

Qiao Jiang

Dr. Qiao Jiang is a Professor in Professor Baoquan Ding's group at the National Center for Nanoscience and Technology (NCNST), where her research focuses on functional DNA nanostructures and their applications in drug delivery. We offer our sincere congratulations to Nanoscale Horizons on its 10th anniversary. We are honored to contribute this manuscript to the special collection, building on our group's recent review published earlier this year. We greatly respect the journal's significant role in publishing high-impact research and look forward to continued success and collaboration within this distinguished community.

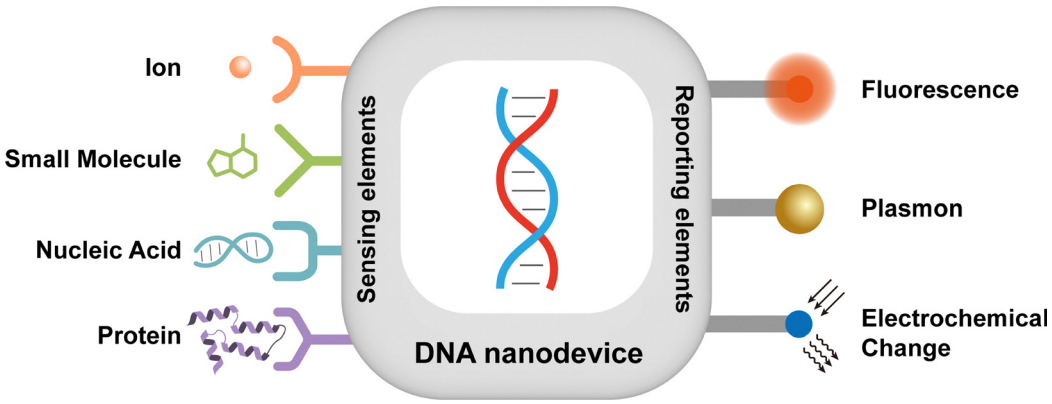

Fig. 1 The general design of self-assembled DNA nanodevices for biosensing.

parameters to identify a targeted molecule could be attached to a single DNA-based biosensor scaffold to improve discrimination. After recognition, reporting elements can transduce the initial binding event into a detectable signal. Fluorophores and nanoparticles, when integrated into DNA scaffolds, are employed to convert the binding of target analytes to sensors into optical and/or electrochemical signals for subsequent analysis.[45,46]

To achieve highly sensitive detection of trace analytes, signal processing and amplification strategies are often integrated into the DNA nanodevices. Techniques such as rolling circle amplification (RCA), hybridization chain reaction (HCR), and catalytic hairpin assembly (CHA) can be incorporated into these platforms to facilitate the detection of low-concentration molecular analytes.[47–49] Additionally, plasmonic enhancement has been employed to improve sensitivity,[50,51] and DNA-assembled plasmonic nanostructures have gained significant attention. These hybrid platforms take advantage of the precise spatial organization of noble metal nanoparticles to exploit unique physicochemical properties, such as plasmonic coupling effects from localized surface plasmon resonance (LSPR). By converting molecular binding events into quantifiable signals, these self-assembled DNA nanodevices enable the sensitive detection of a wide range of molecular targets, including ions, small molecules, nucleic acids, and proteins.

3. Advances in self-assembled DNA nanodevices for efficient biosensing of various analytes

In recent decades, a wide array of self-assembled DNA nanodevices have been developed and successfully applied to biosensing diverse analytes, including ions, small molecules, nucleic acids, and proteins. By harnessing the intrinsic chemical and biological properties of these targets, researchers have designed versatile self-assembled DNA nanoplatforms that integrate customized molecular probes with functional reporting elements. These modular designs not only broaden the spectrum of detectable analytes but also enhance both sensing efficiency and specificity. A representative summary of these systems, including the analytes, probing elements, and reporting strategies, is provided in Table 1, showcasing the breadth and versatility of current biosensing platforms based on self-assembled DNA nanodevices.

Building on this overview, the following sections will provide a more detailed discussion of representative examples, exploring how different DNA nanostructures and sensing mechanisms have been strategically integrated to achieve sensitive and selective detection across various classes of analytes.

3.1. Ion sensing

Ions play a crucial role in numerous biological processes, including signal transduction and cell metabolism.[52–54] While traditional methods for ion sensing relied on macrocyclic fluorescent probes,[42] recent advances have shifted toward functional nucleic acids that selectively bind specific ions. For example, the i-motif interacts with H^+,[38] the G-quadruplex binds to Na^+ and K^+,[37] and various DNAzymes utilize specific metal ions as catalytic centers.[40] These unique properties make functional nucleic acids highly effective components for developing ion sensors.

The precise monitoring of lysosomal ion dynamics such as H^+, Cl^- and Ca^{2+} is important for diagnosing metabolic disorders.[55–57] Recently, Zou *et al.* developed a DNA tetrahedron-based ratiometric fluorescent probe for the simultaneous detection of H^+, Cl^- and Ca^{2+} in lysosomes.[58] The probe is constructed from four single-stranded DNA strands, each functionalized with a specific ion-sensitive fluorophore or a reference fluorophore (Cy5). The rigid DNA tetrahedron framework ensures fixed stoichiometry and spatial separation of fluorophores at its four vertices, enabling precise ratio-based sensing. This probe successfully differentiated these ions with high sensitivity in living cells, resolving lysosomes into distinct subpopulations. To specifically monitor pH dynamics in lysosomes, Yue *et al.* designed a split i-motif with two parts, allowing for tunable pH transition midpoints and signal-to-noise ratios.[59] This system was integrated into a DNA tetrahedron for enhanced stability, cellular uptake, and lysosomal targeting. The optimal nanosensors effectively differentiated

Table 1 A representative summary of biosensing platforms based on self-assembled DNA nanodevices

Category	Analyte	Probing element	Reporting element	Sensing performance	Sensing level	Amplification	Ref.
Ion	H^+	Rosamine derivative (Pr-pH)	Pr-pH and Cy5 (reference)	Sensing range, pH 4.25–5.75	*In vitro*, lysosome	No	58
	H^+	i-Motif	AF546 (donor) and AF647 (acceptor)	Sensing range, pH 5.5–6.5	*In vitro*, lysosome	No	114
	Cl^-	Lucigenin derivative (Pr-Cl)	Pr-Cl and Cy5 (reference)	Sensing range, 0.5–100 mM	*In vitro*, lysosome	No	58
	Cl^-	Biacridinium derivative (BAC)	BAC and AF647 (reference)	Sensing range, 5–120 mM	*In vitro*, lysosome	No	114
	Ca^{2+}	BAPTA derivative (Pr-Ca)	Pr-Ca and Cy5 (reference)	Sensing range, 1–1000 μM	*In vitro*, lysosome	No	58
	Na^+	1-Aza-15-crown-5 ether derivative (Chicago Green)	Chicago Green and ATTO647N (reference)	Sensing range, 5–145 mM	*In vitro*, lysosome	No	62
	K^+	TAC-Rhodamine derivative (TAC-Rh)	TAC-Rh; AF488 (donor)-modified i-motif and AF647 (acceptor) for pH correction	Sensing range, 0.1–140 mM	*In vitro*, *trans*-Golgi network, early and recycling endosomes	No	64
	Zn^{2+}	Zn^{2+}-dependent DNAzyme	Cy3 (donor) and Cy5 (acceptor)	Sensing range, 0.5–10 μM; LoD, 345 nM	*In vivo*	No	66
	Hg^{2+}	T-rich strand	Cy3	LoD, 10 nM; reaction time, 5 min	Water sample	No	69
	Hg^{2+}	T-rich Mg^{2+}-dependent DNAzyme	FAM and MOF quencher	LoD, 0.11 nM	Water sample	No	110
	Ag^+	C-rich strand	Cy3	LoD, 10 nM; reaction time, 5 min	Water sample	No	69
	Ag^+	C-rich Mg^{2+}-dependent DNAzyme	TAMRA and MOF quencher	LoD, 0.25 nM	Water sample	No	110
	Pb^{2+}	Pb^{2+}-dependent DNAzyme	Cy3	LoD, 20 nM; reaction time, 5 min	Water sample	No	69
	Ni^{2+}	Ni^{2+}-dependent DNAzyme	ROX and MOF quencher	LoD, 7.8 μM	Water sample	No	110
Small molecule	ATP	ATP aptamer	Cy5	Sensing range, 50–500 μM	*In vivo*, tumor microenvironment	No	76
	ATP	ATP aptamer	Cy5 and BHQ2 quencher	Sensing range, 1–8 mM	*In vivo*, mitochondria in tumor cell	No	78
	GSH	Disulfide bond	Cy5 and BHQ2 quencher	Sensing range, 1–8 mM	*In vivo*, mitochondria in tumor cell	No	78
	Glucose	Glucose oxidase and i-motif	Cy5.5 and BHQ3 quencher	Sensing range, 50 mg dL^{-1}–400 mg dL^{-1}; accuracy, 98.70 ± 4.77%	*In vivo*, skin	No	79
	Cocaine	Cocaine aptamer	Gold electrode	Sensing range, 10^{-11}–10^{-5} M	Solution	No	80
	L-Tyrosinamide	L-Tyrosinamide aptamer	Gold nanorod	LoD, 10 μM	Solution	CHA	102
Nucleic acid	SARS-CoV-2 RNA	Complementary DNA	Graphene field-effect transistor	LoD, 0.02 copies per μL	Nasopharyngeal swab sample	No	81
	SARS-CoV-2 RNA	Complementary DNA	Multi-arm DNA nanostructure and quartz nanopore	LoD, CT value = 20	Oropharyngeal swab sample	No	109
	Mature miR-21	Complementary DNA	Cy5 and BHQ3 quencher	LoD, 2.05 fM; accuracy, 90%	Serum sample	Thermophoresis	84
	miR-21	Complementary DNA	Cy3 (donor) and Cy5 (acceptor)	LoD, 2 nM	*In vitro*, cytoplasm	CHA	85
	miR-21	Complementary DNA	Cy5 and BHQ3 (quencher and photoacoustic imaging contrast)	Sensing range, 1.5–80 nM	*In vivo*, kidney	No	118
	miR-155	Complementary DNA	Cy3 (donor) and Cy5 (acceptor)	LoD, 1 nM	*In vitro*, cytoplasm	CHA	85
	miR-221	Complementary DNA	FAM and BHQ1 quencher	Sensing range, 5 pM–50 nM	*In vitro*, cytoplasm	RCA, HCR	99
	miR-222	Complementary DNA	Cy5 and BHQ2 quencher	Sensing range, 5 pM–5 nM	*In vitro*, cytoplasm	RCA, HCR	99
	TK1 mRNA	Complementary DNA	Cy3 and BHQ2 quencher	LoD, 200 pM	*In vitro*, cytoplasm	No	87
	iNOS mRNA	Complementary DNA	Cy5 and BHQ2 quencher	Sensing range, 8.8 pM–100 nM	*In vivo*, ankle joint and kidney	HCR	100
Protein	SARS-CoV-2 spike protein	Spike protein aptamer	FAM and BHQ1 quencher	LoD, 10^3 copies per mL; reaction time, 10 min	Saliva sample	No	95
	SARS-CoV-2 spike protein	Spike protein aptamer	FAM and BHQ1 quencher	LoD, 10^2 copies per mL; reaction time, 10 min	Saliva sample	Photonic crystal enhanced fluorescence	96
	Cardiac troponin I (cTnI)	cTnI antibody	Gold nanoparticle	LoD, 2 pM	Serum sample	No	97

Table 1 (*continued*)

Category	Analyte	Probing element	Reporting element	Sensing performance	Sensing level	Amplification	Ref.
	VEGF	VEGF aptamer	Cy3 and BHQ2 quencher	LoD, 32.4 ng mL^{-1}	*In vitro*, tumor cell membrane	No	98
	Monkeypox viral antigen A35R	A35R antibody clon 19 and clon 43	Carbon nanotube field-effect transistor	LoD, 991 aM	Solution	No	101
	Streptavidin	Biotin	Raman peaks of streptavidin	Sensing range, 330 nM–4.2 μM	Solution	Surface-enhanced Raman scattering	105
	Thrombin	Thrombin aptamer (HD22)	Raman peaks of thrombin	Sensing range, 6.9–61 μM	Solution	Surface-enhanced Raman scattering	105
	Anti-digoxigenin antibody	Digoxigenin	ATTO542 (donor) and ATTO647N (acceptor)	LoD, 103.5 pM	Solution	Single-molecule confocal microscopy	106
	PDGF-BB	PDGF-BB aptamer	ATTO542 (donor) and ATTO647N (acceptor)	LoD, 100 pM	Solution	Single-molecule confocal microscopy	106
	OVA-specific TCR	H-2K^b MHC with OVA peptide	PE	Affinity, cell K_d = 1.8 nM; Sensing efficiency, 99.3% of positive cells	Blood sample	No	112
	EpCAM, EGFR and HER2 on MCF-7 cell	EpCAM aptamer, EGFR aptamer and HER2 aptamer	Cy5	Affinity, cell K_d = 263.9 ± 0.6 pM; Sensing efficiency, 17–214 cells per mL	Blood sample	No	113
	Kim-1	Kim-1 targeting ligand	Cy7 or gold nanoparticle	Affinity, cell K_d = 25.26 nM	*In vivo*, kidney	No	120

lysosomes from early endosomes and successfully visualized pH fluctuations in living cells, providing a valuable platform for exploring lysosomal biology and disease diagnostics.

Na^+ and K^+ ions are essential for maintaining cellular function, particularly electrochemical signaling and cellular homeostasis.[60,61] The asymmetrical distribution of Na^+ across the plasma membrane drives molecular transmembrane transport, however, the establishment of corresponding gradients at the organellar level remains less clear. To investigate this, Zou *et al.* created a DNA nanodevice for Na^+-sensing in endocytosis-related organelles.[62] This DNA nanodevice incorporated a pH-insensitive Na^+-reporting fluorophore named Chicago Green, a reference dye, and an organelle-targeting domain within a DNA duplex. In living mammalian cells and *C. elegans*, the sensors mapped Na^+ characteristics at a single endosome resolution, revealing that Na^+ concentration declined during the endocytosis process due to the activation of two-pore channels and Na^+/H^+ exchangers.

The K^+ gradient is intricately linked to the Na^+ gradient, with both collectively serving as a primary driving force for molecular transmembrane transport.[63] However, the accurate quantification of K^+ in acidic environments remains challenging due to the pH sensitivity of the macrocyclic ligands used for its specific recognition. To address this issue, Anees *et al.* developed a DNA-based pH-correctable, ratiometric intracellular K^+ reporter.[64] This three-way DNA junction contained a pH-responsive i-motif and a K^+-sensitive dye for simultaneous measurement of organellar pH and K^+ levels, allowing for pH correction. These DNA reporters successfully targeted early endosomes, recycling endosomes, and the trans-Golgi networks, revealing that luminal K^+ levels in recycling endosomes increased with wild-type Kv11.1 channel expression.

Zn^{2+} is another essential abundant metal ion, and its abnormal accumulation in organelles is linked to cellular dysfunction.[65] Using high-intensity focused ultrasound (HIFU) techniques, Wang *et al.* developed a noninvasive, spatiotemporally controlled method for DNAzyme-based Zn^{2+} imaging *in vivo* (Fig. 2a).[66] The Zn^{2+}-selective DNAzyme probe was initially blocked by a protector strand. In the presence of HIFU-induced localized heating, the probes were activated by de-hybridization of the protector strands. With this design, the probes showed minimal fluorescence resonance energy transfer (FRET) signals before HIFU and increased fluorescence after activation in both HeLa cells and mice. This external field-controlled strategy offered a promising tool for the investigation of metal ion dynamics *in vivo*.

Heavy metal ions, such as Hg^{2+}, Ag^+ and Pb^{2+} ions, have been recognized as important environmental pollutants, which are toxic and hazardous to human health.[67,68] For on-site environmental monitoring, Qu *et al.* developed a DNA nanostructure microarray within a microchannel platform to detect heavy metal ions.[69] Tetrahedral DNA structures containing target-specific probes, including thymine (T)-rich sequences for the selective coordination with Hg^{2+}, cytosine (C)-rich oligonucleotides for the interaction with Ag^+, and a DNAzyme for specific Pb^{2+} recognition, were assembled and immobilized

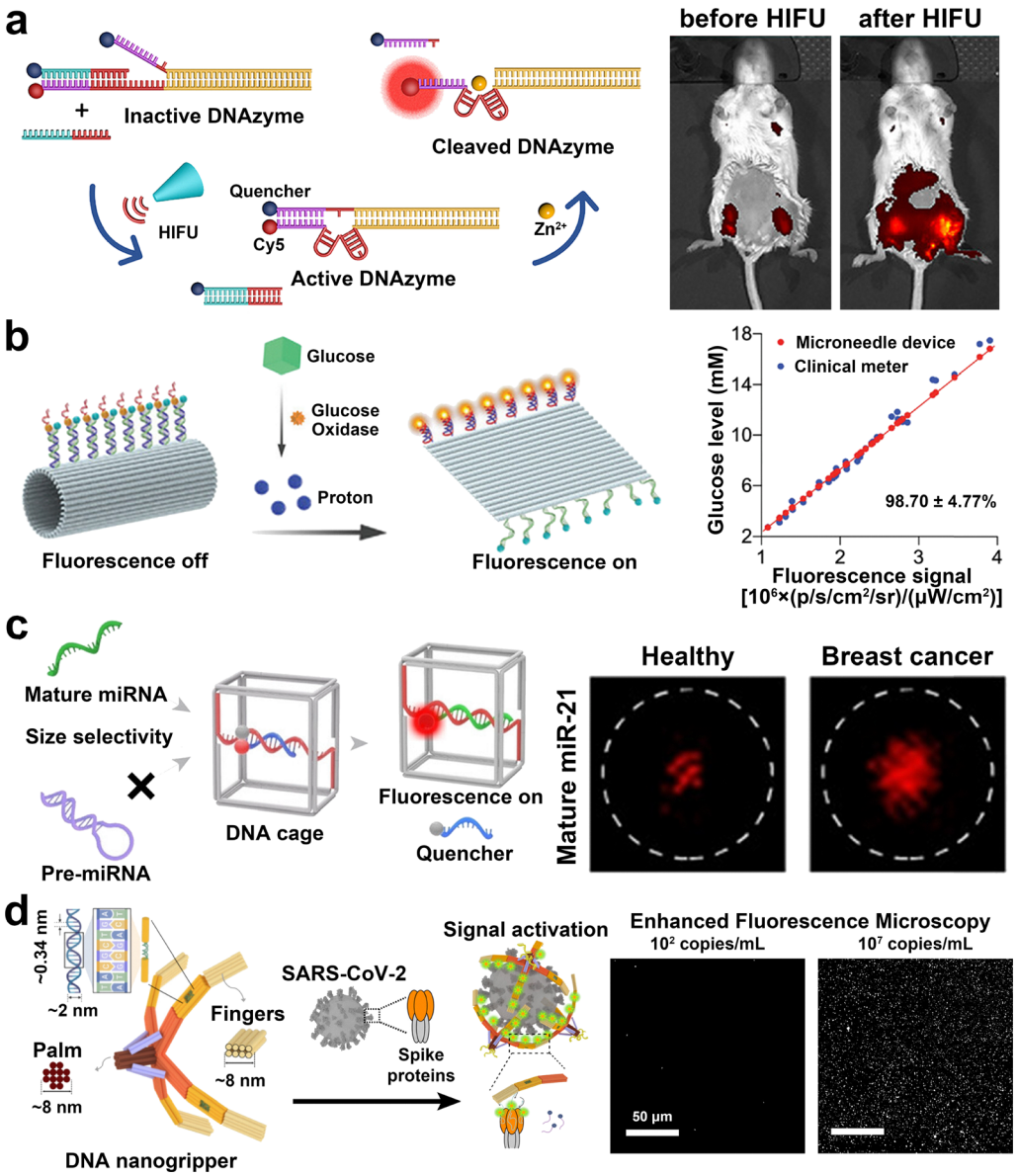

Fig. 2 Self-assembled DNA nanodevices for efficient biosensing of various analytes. (a) HIFU-activated DNAzyme probe for *in vivo* Zn^{2+} imaging. Reproduced with permission from ref. 66. Copyright 2022, American Chemical Society. (b) DNA origami nanodevice for blood glucose monitoring. Reproduced with permission from ref. 79. Copyright 2023, John Wiley and Sons. (c) DNA cage for selective sensing of mature miRNA. Reproduced with permission from ref. 84. Copyright 2023, John Wiley and Sons. (d) DNA nanogripper for spatial recognition of viruses. Reproduced with permission from ref. 96. Copyright 2024, AAAS.

along the microchannels. In the presence of individual metal ions, the specific fluorophore-labeled reporter strands in the aqueous solution can be captured, generating corresponding fluorescent signals for each pollutant.

3.2. Small molecule sensing

Small molecules, such as glucose and ATP, are crucial for cellular function and signal transduction, making them valuable diagnostic biomarkers.[70–72] Chemically synthesized nucleic acids like DNA/RNA aptamers and disulfide bond-modified oligonucleotides can selectively bind to specific targets and are readily integrated into self-assembled DNA nanodevices for small molecule sensing.

A tumor microenvironment (TME) is characterized by significantly elevated ATP concentrations, typically 10^3 to 10^4 times higher than in healthy tissues, making it a key biomarker for tumorigenesis.[73–75] Ai *et al.* reported a tunable DNA nanocircle for the sensing of ATP, where an ATP-binding aptamer was split into two segments and embedded between two protein tyrosine kinase 7 (PTK7)-targeting aptamers.[76] The nanocircle remained inactive under normal conditions but underwent a conformational switch only when it encountered both the PTK7 marker of specific tumor cells and elevated local ATP concentrations in the TME.

In addition, elevated glutathione (GSH) levels in tumor cells have been implicated in facilitating tumor progression,

correlating with the level of ATP.[77] Chai *et al.* designed a redox-activatable ATP aptamer sensor for mitochondria-targeted imaging.[78] The assembled sensor, loaded onto cationic polymer nanoparticles, consisted of a fluorophore-labelled ATP aptamer and a quencher-tagged complementary blocker strand modified with a disulfide bond at a specific site. In the presence of GSH, the blocker strand was cleaved, reducing its binding affinity with the ATP aptamer. When ATP was present, the fluorophore-labelled aptamer underwent a conformational change and dissociated from the blocker strand, thereby restoring the fluorescence signal and achieving correlated imaging of GSH and ATP in tumor cells.

Quantitative blood glucose monitoring is critical for diabetes management, however, current methods typically involve invasive blood sample collection, which can cause tissue damage and the risk of infection. To address this, Li *et al.* developed a DNA origami-incorporated microneedle device for *in situ* glucose monitoring (Fig. 2b).[79] The device was constructed by fabricating DNA origami nanosheets, which were sealed with multiple proton-sensitive DNA fasteners. Cy5 dyes and black hole quencher 3 (BHQ3) were incorporated as FRET pairs, allowing the DNA tubular structures to remain in a quenched state. These DNA tubes and glucose oxidase molecules were further physically trapped in the methacryloyl hyaluronic acid (mHA)-based inner-core network of the microneedles. When the microneedle device was applied to the skin, glucose-containing interstitial fluids were collected *in situ*. The glucose in the fluid was catalyzed by glucose oxidase to produce protons. Localized within the needles, the protons triggered a conformational change of the DNA nanotubes, resulting in fluorescence emission. This painless, transdermal device converted glucose into H^+ by reconfiguring DNA origami to amplify fluorescence, showing 98.70% accuracy in clinical tests. The devices offered an encouraging, less invasive, and highly sensitive strategy for real-time blood glucose monitoring.

Continuous, real-time monitoring of cocaine is crucial for clinical and forensic applications. Chen *et al.* designed a regeneratable cocaine-sensing system that combined anti-cocaine aptamer with pH-sensitive DNA strands.[80] The pH-sensitive DNA sequence, which can change its configuration from a duplex to a triplex in the presence of protons, was incorporated into an anti-cocaine aptamer. These thiolated, pH-sensitive aptamers were modified onto gold electrodes to create a DNA-functionalized surface as an electronic sensing platform for cocaine. In their study, cocaine molecules were captured and detected by the aptamer-mediated sensing electrode. After the cocaine was captured, a mild acidic solution was introduced, causing the protons to trigger the duplex-to-triplex conformational change of the pH-sensitive strands, which in turn released the bound cocaine molecules from the aptamer-coated electrode surface. This design not only enabled specific cocaine sensing but also provided a method for *in situ* sensor regeneration under mild, biocompatible conditions.

3.3. Nucleic acid sensing

Nucleic acids, such as viral genomes, miRNA, and mRNA, are crucial biomarkers for biosensing, particularly in pathogen detection and cancer diagnosis. Beyond traditional polymerase chain reaction (PCR) techniques, synthetically engineered DNA-assembled nanodevices provide rapid, sensitive, and isothermal alternatives for detecting these biomarkers. These devices leverage rationally designed complementary probes and strand displacement reactions to achieve efficient detection.

In the battle against epidemics, rapid and sensitive detection of viral genomes remains a critical challenge. Wang *et al.* developed a novel electromechanical biosensor for ultrasensitive detection of SARS-CoV-2 RNA.[81] They designed a molecular system consisting of a rigid tetrahedral DNA nanostructure and a flexible ssDNA probe extended from the vertex with a sequence complementary to the target viral RNA. The DNA tetrahedron was covalently linked to anchor molecules (1-pyrenebutanoic acid succinimidyl ester, PASE), which were previously immobilized onto the graphene transistor *via* π–π stacking to avoid non-specific interactions between the DNA structures and the graphene layer. When a negative gate voltage was applied, the local electrical field actuated the cantilevers downwards, bringing them closer to the graphene surface. This increased the interaction between the analytes and the graphene layer. These binding events altered the electrical properties of the graphene channel, causing a detectable current response. This platform enabled ultrafast and ultrasensitive detection of SARS-CoV-2 RNA in patient samples, without RNA extraction and amplification procedures required for a traditional quantitative reverse transcription-polymerase chain reaction (qRT-PCR) approach.

MicroRNAs (miRNAs) are a class of non-coding small RNA molecules (19–25 nucleotides) whose abnormal expression is closely correlated with the onset and metastasis of various cancers.[82,83] For the *in situ* detection of mature miRNA in extracellular vesicles (EVs), Zhao *et al.* developed a DNA cage-based thermophoretic assay (Fig. 2c).[84] They designed a DNA cage structure consisting of a nanoscale DNA framework, a Cy5-labeled recognition sequence (F), and a quencher-tagged complementary strand (Q). After incubation with EVs, the encapsulated DNA frameworks allowed only mature miRNA, which is shorter in length, to enter the confined cavities. There, the miRNA hybridized with the recognition sequence, recovering the fluorescence signal. Polyethylene glycol (PEG) was added to serum samples to enhance thermophoretic accumulation of EVs for amplification of the fluorescence signal. The approach achieved a selective, *in situ* detection of mature miRNAs in EVs with a limit of detection (LoD) of 2.05 fM.

An enzyme-free catalytic hairpin assembly strategy has also been explored for the formation of constitutional dynamic networks (CDNs) and miRNA sensing. Zhou *et al.* designed a spatially localized DNA circuit for miRNA sensing.[85] The circuit was composed of a DNA tetrahedron functionalized at its corners with DNA anchors to form an entropy-driven DNA circuit, followed by the dynamic assembly of the CDNs. In the presence of miR-21 and miR-155, specific conformational changes occurred in the localized DNA circuits, resulting in different FRET intensities for sensing.

Messenger RNAs (mRNAs) that encode key proteins involved in pathological signaling pathways can also serve as valuable biomarkers for disease assessment.[86] Ma *et al.* engineered a

DNA tile-based assembly to serve as a biosensor for simultaneous visualization of TK1 mRNA and synergistic cancer killing.[87] A four-arm DNA tile was fabricated and then functionalized with a self-quenched molecular beacon (MB) containing a 17-nt recognition sequence that targeted TK1 mRNA in the cytoplasm. I-motifs and aptamer components were introduced into the DNA tiles to form intermolecular structures under extracellular acidic pH, and to enhance target affinity, cellular uptake, and membrane permeability of the DNA assemblies. Once internalized, the MBs hybridized with TK1 mRNA, restoring their fluorescence for precise imaging and simultaneously inducing gene silencing. Additionally, these GC-rich DNA scaffolds were loaded with doxorubicin for cellular delivery and controlled intracellular release, providing a cooperative effect of combined gene and chemotherapeutic therapies. This integrated, stimuli-responsive nanoplatform offers a versatile and efficient approach for cancer theranostics.

3.4. Protein sensing

Proteins are essential biomolecules that drive critical life processes and maintain cellular integrity and metabolic function. In pathological states, alterations in protein expressions or structures are frequently associated with disease onset and progression.[88–91] Proteins are therefore key targets for disease diagnosis and pathogen detection. In addition to traditional techniques such as enzyme-linked immunosorbent assays (ELISA), western blotting and surface plasmon resonance (SPR),[92–94] self-assembled DNA nanodevices offer a novel approach for protein detection by integrating aptamers, antibodies, and peptide ligands, enabling the precise identification and quantification of disease-associated protein biomarkers.

The COVID-19 pandemic highlighted the need for rapid, sensitive, and accessible methods for viral antigen detection and inhibition. Chauhan *et al.* designed flexible, net-shaped DNA-based nanosensors for recognizing antigen proteins and capturing intact SARS-CoV-2 virions.[95] A series of wireframed DNA net nanostructures with different sizes were constructed, and subsequently functionalized with multiple copies of fluorescence dye-tagged aptamers that specifically recognize the receptor binding domain (RBD) of SARS-CoV-2 spike proteins. These aptamers were precisely organized by the DNA nets, forming trimeric cluster arrays to mechanically match trimeric spike protein patterns on the viral surface. Quencher-attached ssDNA locks that were partially complementary to the aptamers were hybridized and used to quench the fluorescence reporters, forming the sensing motifs of the DNA nets. When the DNA net sensors bound to the virus, the lock DNA strands were displaced from the net's sensing motifs, activating their fluorescence output. This DNA net sensor achieved a rapid and sensitive detection of SARS-CoV-2 virions, with an LoD of ~1000 copies per mL in artificial saliva, using a portable fluorimeter, with results that were comparable to those of qRT-PCR. Furthermore, the DNA net-aptamer complex showed increased neutralizing potency of virions by blocking the interaction between viral spikes and their receptors, ACE2, expressed on their host cells, indicating the potential to inhibit viral infection in cell culture.

Similar to those flexible DNA nets, the same group created DNA origami-based, robotic nanogrippers with advanced spatial recognition and inhibition capabilities against the SARS-CoV-2 virus (Fig. 2d).[96] Inspired by human hands and bird claws, this DNA origami nanogripper was composed of a central palm (8 nm × 8 nm) and four bendable fingers (approximately 67 nm long). Multiple rotatable joints connected the fingers' phalanges, enabling control of their bending movements for encapsulating virion particles. For specific binding with SARS-CoV-2 virus, the nanogrippers were also incorporated with similar sensing motifs containing aptamer-based reporter-quencher pairs, generating fluorescence signals for viral detection. The DNA nanogrippers captured virions when anchored to a photonic crystal surface, enabling the detection of SARS-CoV-2 in human saliva with an LoD of ~100 copies per mL. Additionally, the DNA nanogrippers demonstrated inhibition of viral entry into host cells, suggesting the potential in anti-infection treatment. These advances present promising DNA nanodevice-based platforms for both ultrasensitive viral diagnostics and potential antiviral therapeutics.

Self-assembled DNA nanodevices can also act as signal amplifiers in immunoassays, improving diagnostic efficacy. Ijäs *et al.* used a DNA origami six-helix bundle (8 nm × 490 nm) as a molecular adapter to connect a small amount of specific detection antibodies to a large number of signal-generating labels, such as 40-nm gold nanoparticles or AF647-DNA.[97] In this amplified system, the increased number of labels per antibody and per bound analyte resulted in a stronger signal, making trace analyte concentrations detectable. By controlling origami structure design, label types and the ratio of labels to antibodies, the amplification factors of the sensing system can be adjusted, ranging from one to several hundred, to meet the desired sensitivity for signal-amplified lateral flow immunoassays (LFIAs). The authors further incorporated this sensing origami system into a conventional LFIA test strip, which was composed of a nitrocellulose membrane striped with capture reagents (*e.g.*, antibodies or streptavidin) and pads for sample and buffer application. For the detection of cardiac troponin I, a key biomarker for cardiovascular diseases, in human serum sample, this system achieved a LoD of 1.5 pM within 15 minutes. In comparison with gold particles as labels, which showed 55-fold improved assay sensitivities, fluorescence labels displayed tailored amplification up to 125-fold.

DNA nanodevice-based biosensors have also emerged as valuable tools for biological studies in cellular signaling. Chen *et al.* designed multi-tasking, Y-shaped DNA structures that can sense and regulate the hepatocyte growth factor (HGF)/cellular mesenchymal-epithelial transition (c-Met) signaling and subsequent vascular endothelial growth factor (VEGF) secretion located on the cell membrane.[98] This DNA device featured three functional modules: a cholesterol-tagged DNA duplex for cell membrane anchoring, a MB incorporating VEGF aptamer and Cy3 dye for cellular signal reporting, and a photo-responsive PC linker, c-Met aptamer and Cy5 dye-containing strands for

inhibiting HGF/c-Met signaling upon light irradiation. Without light, HGF treatment induced dimerization and activation of c-Met receptors expressed on HeLa cell membranes, resulting in cellular VEGF production, and subsequent secretion out of the cell. These secreted VEGF molecules around the cell membrane were recognized by the DNA devices, which released the quenched strands of the MBs and activated Cy3 fluorescence on the membrane. Upon light irradiation, the PC-linker was cleaved, unblocking the c-Met aptamer and forming the active conformation, which served as an inhibitor to bind with the c-Met receptor monomer and turned on Cy5 signals on the cell surface. This DNA device demonstrated enhanced, controllable c-Met inhibition and real-time monitoring of related VEGF changes, providing a versatile tool for studying receptor-mediated signaling pathways in living cells.

4. Engineering self-assembled DNA nanodevices for intelligent biosensing

The increasing demands for advanced biosensing techniques in biomedical diagnostics and biological research have spurred the development of sophisticated platforms. In response, researchers have harnessed the inherent programmability and addressability of self-assembled DNA nanoplatforms to engineer intelligent nanodevices. These DNA nanodevices are no longer limited to simple detection; they integrate multiple sensing functions, perform logic-gated signal processing, respond to complex microenvironments, and amplify signals to enhance sensitivity. Such versatility has led to significant advancements in ultrasensitive detection, multiplexed sensing, and targeted molecular bioimaging, thereby broadening the scope of modern biosensing strategies.

4.1. Ultrasensitive detection

To achieve a lower limit of detection (LoD) in biosensing, various sensitivity-enhancing strategies have been employed in construction of self-assembled DNA nanodevices. Two primary strategies, signal amplification and single-molecule sensing, have been widely applied, both enabling significant improvements in detection capabilities. Signal amplification techniques, such as isothermal amplification methods of nucleic acids (like RCA, HCR, and CHA), have been extensively used to boost sensitivity. Additionally, electrochemical transducers and plasmonic nanoparticles have been integrated with nucleic acid probes to convert and amplify molecular binding events into detectable electrical or optical signals. In contrast, single-molecule sensing techniques bypass ensemble averaging, enabling the direct observation of individual biomolecules and thereby achieving ultrasensitive performance.

Building on amplification-based strategies, researchers have developed DNA nanostructures for sensitive *in situ* quantification of low-abundance intracellular biomarkers such as microRNA and mRNA. Zhou *et al.* designed a DNA nanostructure-based miRNA sensing and amplifying platform,[99] in which a tetrahedral DNA framework was modified with locked primers. When the target miRNAs were present, a toehold-mediated chain displacement reaction was triggered, releasing the primers. The exposed primers initiated RCA reactions, generating long DNA strands with interval sequences as initiators to trigger subsequent HCRs. This process formed supramolecular DNA networks and recovered the fluorescent signals from quenching, enabling sensitive detection and intracellular imaging of dual miRNAs and helping to distinguish liver cancer cells with different metastatic potentials. As another example, Jia *et al.* employed a DNA origami platform modified with HCR probes for imaging inflammation-related mRNA (Fig. 3a).[100] The HCR component strands, including mRNA-sensing sequences, were precisely preorganized on a triangular origami with finely tuned distances, numbers, and patterns. The presence of mRNA segments of inducible nitric oxide synthase (iNOS), a marker for inflammation, initiated HCR and recovered fluorescence signals. This origami-based HCR imaging technique realized early-stage diagnosis of acute inflammation in mouse models of gouty arthritis and sepsis-associated kidney injury.

Beyond nucleic acid amplification, weak biomolecular interactions can also be transduced into amplified electrochemical outputs. For instance, Ren *et al.* developed a tetrahedral DNA-based electrochemical nanodevice to identify monkeypox virus antigen proteins.[101] They used tetrahedral DNA nanostructures (TDNs) as scaffolds to precisely arrange two antibodies of A35R antigen for multivalent recognition. These antibody-TDNs were attached to an electrolyte-gated carbon nanotube (CNT) field-effect transistor (EG-FET), forming the virus-sensing devices. By integrating the specific binding of the antibody-TDNs with the electrical properties of the CNT-FET, this biosensing system achieved the detection of a trace amount of the A35R antigen, with a LoD of 991 aM.

For optical signal amplification, Liu *et al.* developed a DNA origami-based plasmonic nanodevice to sense and magnify trace molecular signals (Fig. 3b).[102] They constructed a tweezer-like DNA origami nanostructure as a template for arranging gold nanorod (GNR) into an asymmetric conformation that produced a chiral plasmonic circular dichroism (CD) signal. Folding strands as controlling elements were assembled to connect the two tweezer arms and hold the plasmonic nanodevice into a closed state. When target molecules were present, the controlling elements triggered a conformational change, transitioning the whole structure into an open state and separating the GNRs on the two arms of the DNA origami tweezers. This structural reconfiguration was converted into plasmonic CD signals, realizing the detection of corresponding small-molecular analytes.[103] A DNA logic circuit to recognize and amplify weak biological signals was further involved, enabling the identification of trace amounts of small biomolecules, such as adenosine and L-tyrosinamide.[104] This versatile platform offers a sensitive way to detect biological signals through controlled structural motions and optical readouts.

In addition to amplification strategies, single-molecule approaches provide a direct route to ultrasensitive detection. For instance, Schuknecht *et al.* constructed DNA origami-based

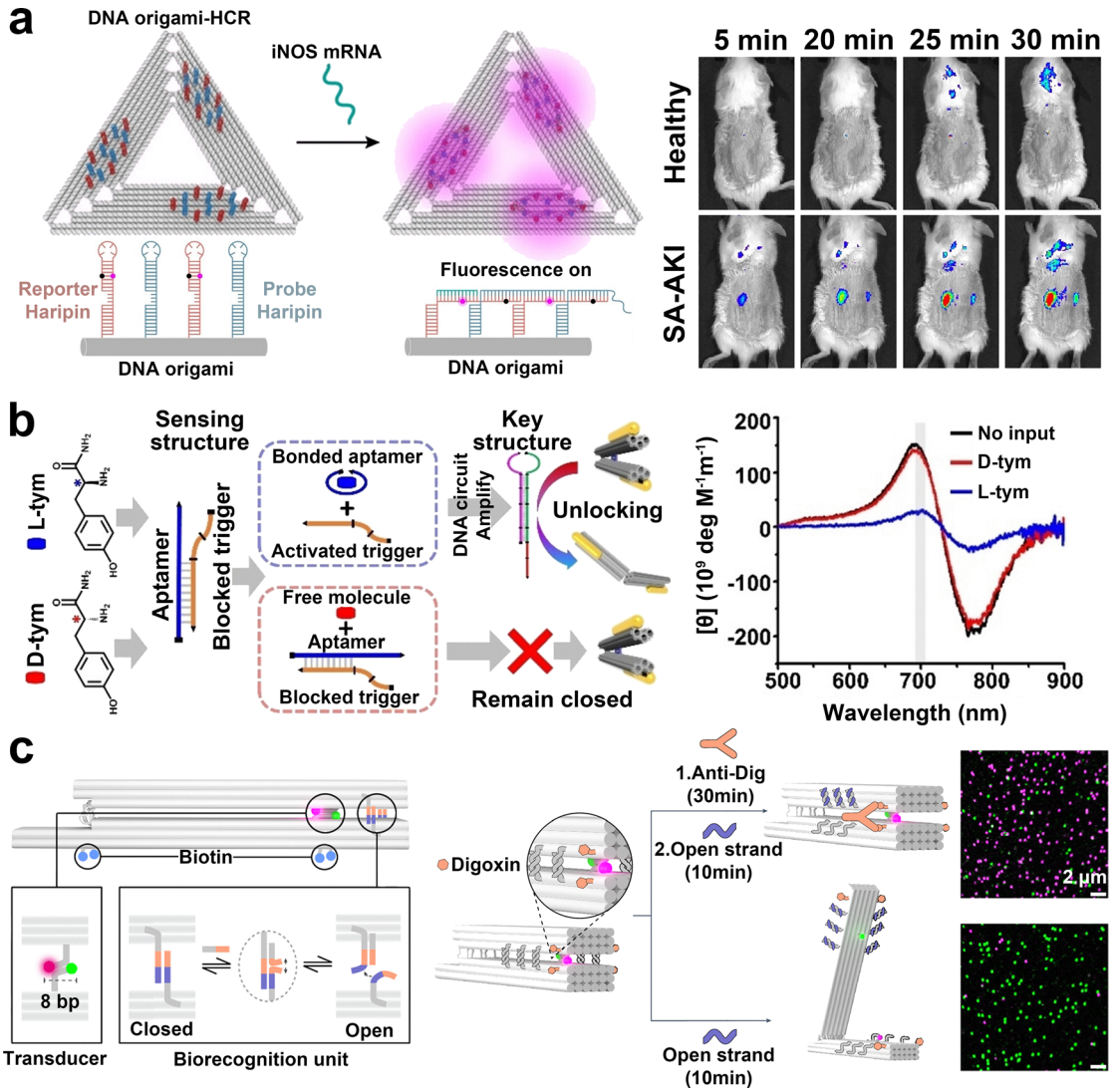

Fig. 3 Self-assembled DNA nanodevices for ultrasensitive detection. (a) HCR probe-modified DNA origami for intracellular mRNA imaging. Reproduced with permission from ref. 100. Copyright 2024, John Wiley and Sons. (b) DNA origami-based plasmonic nanodevice for L-tyrosinamide sensing. Reproduced with permission from ref. 102. Copyright 2022, John Wiley and Sons. (c) Dynamic DNA origami platform for single protein sensing. Reproduced with permission from ref. 106. Copyright 2025, Spinger Nature.

plasmonic nanoantennas for label-free single-protein detection.[105] They constructed a DNA origami tube with extended capture stands, guiding GNRs modified with complementary ssDNA to the pre-designed sites. On each origami tube, a GNR dimer was organized in a tip-to-tip configuration, creating an interparticle gap (~8 nm wide) as a plasmonic hotspot. Specific DNA anchor strands were positioned within these hotspots to capture target proteins in the solution. The assembled nanoantennas provided sufficient surface-enhanced Raman scattering (SERS) enhancement, enabling the label-free detection of individual streptavidin and thrombin molecules with sub-second integration times.

In another example, Grabenhorst *et al.* presented a dynamic DNA origami nanostructure incorporated with FRET pairs for optical signal responses (Fig. 3c).[106] They designed a hinged DNA origami capable of undergoing large conformational changes. Donor (ATTO542) and acceptor (ATTO647N) dye molecules were located on the opposite surface of the two arms of the origami structure, forming a FRET pair as a signal transduction element. On the DNA hinge templates, DNA overhangs were designed to sense the specific triggers and control the two arms to open or close. In the closed state, the dyes of FRET pairs were held together by the two approximated DNA arms and weak 8-bp DNA hybridization, allowing for energy transfer and a FRET signal. When the triggers interacted with the controlling overhangs, the closed structures unfolded, separating the dye molecules. The altered FRET signals were quantified by single-molecule confocal microscopy. The modularity of this platform was demonstrated by adapting it to detect various proteins such as anti-digoxigenin antibody, PDGF-BB and XhoI.

Finally, moving toward super-resolution imaging, Schnitzbauer *et al.* introduced DNA-PAINT (DNA-based Point Accumulation for

Imaging in Nanoscale Topography), a super-resolution imaging method utilizing DNA-based probes to overcome conventional localization limits.[107] The technique relies on transient hybridization of dye-labeled "imager" strands with complementary "docking" sequences on target molecules, enabling programmable, sequence-specific labeling independent of fluorophore photophysics. Leveraging the DNA-PAINT technique, Sun *et al.* achieved the localization of proteasome 19S and 20S particles in neuronal subcellular compartments with single-molecule resolution.[108] The modular design and compatibility of this innovative imaging technique position it as a transformative platform for optical nanoscopy, expanding molecular-scale analysis in biological systems.

Taken together, these diverse amplification and single-molecule techniques highlight the versatility of self-assembled DNA nanodevices in pushing the sensitivity limits of biosensing.

4.2. Multiplexed sensing

While ultrasensitive detection is crucial for identifying trace targets, the simultaneous recognition of multiple biomarkers is increasingly required in real-world biomedical diagnostics, enabling precision medicine and personalized treatment. DNA nanotechnology, with its inherent programmability and modularity, enables the integration of multiple sensing and reporting modules into a single platform, thereby advancing multiplexed sensing capabilities.

For instance, Bošković *et al.* created a programmable DNA bait for nanopore-based viral diagnostics (Fig. 4a).[109] The DNA nanobait built on a single-stranded M13mp18 DNA scaffold and hybridized with short oligonucleotides containing capture strands complementary to specific regions of target viral RNA. A partially complementary ssDNA tagged with a protein or DNA-based structural label was added to each capture site as reporters. In the presence of target RNA fragments cleaved from viral RNA by RNase H, the reporter strands can be displaced and released from the nanobait, which then produced specific current signals in a nanopore. The sensing platform enabled not only simultaneous discrimination of multiplexed viral variants but also the identification of multiple sites of SARS-CoV-2 RNA.

In addition to viral detection, multiplexed DNA nanodevices have also been employed for environmental monitoring. Pavadai *et al.* developed a versatile fluorescent biosensing platform

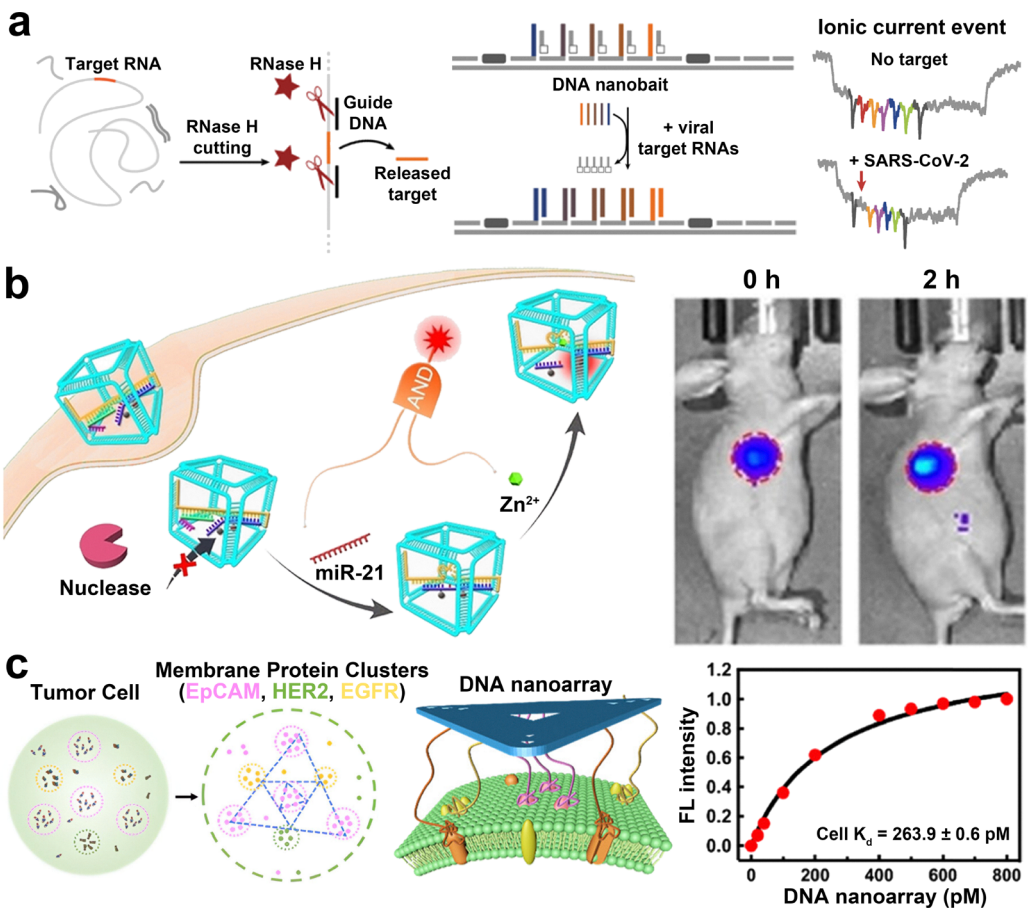

Fig. 4 Self-assembled DNA nanodevices for multiplexed sensing. (a) DNA nanobait for spontaneous detection of multiple viral RNAs. Reproduced with permission from ref. 109. CC BY 4.0 license. Published by Spinger Nature, 2023. (b) DNA nanocage protected DNAzyme sensor for miR-21 and Zn^{2+} imaging in tumor-bearing mice. Reproduced with permission from ref. 111. Copyright 2025, John Wiley and Sons. (c) DNA origami-based aptamer nanoarrays for enhanced capture of circulating tumor cells. Reproduced with permission from ref. 113. Copyright 2023, American Chemical Society.

for simultaneous detection of multiple heavy metal ions (Hg^{2+}, Ni^{2+}, and Ag^{+}).[110] The platform utilized a three-fluorophore-labeled Y-shaped DNAzyme and a metal-organic framework (MOF)-based nanobox as an efficient quencher. In the presence of a particular type of metal ions, the corresponding DNAzyme cleaved its substrate DNA strand, and the cleaved fluorophore-labeled fragments adsorbed onto the MOF surfaces, causing fluorescence quenching. This metal ion sensing platform exhibited high catalytic activity and selectivity, successfully determining multiple heavy metal ions in real water samples.

Beyond simple simultaneous detection, self-assembled DNA nanodevices can perform advanced logic-gated sensing and molecular computation, allowing higher-order analysis of complex biological signals. For example, Tu *et al.* designed a DNAzyme sensor confined within a DNA nanocage for AND-logic imaging of both tumor miRNA and Zn^{2+} ions (Fig. 4b).[111] The DNA nanocages enabled efficient intracellular delivery and steric protection for the functional DNAzymes. These DNAzyme sequences were initially blocked until activated by miR-21-mediated strand displacement in tumor cells. The activated DNAzymes then cleaved the corresponding substrate strands in the presence of Zn^{2+}, releasing the quencher-containing fragment and generating a fluorescence signal output. This system allows AND-logic molecular imaging of both miR-21 and Zn^{2+} with improved precision, successfully monitoring target fluctuations in disease models.

In a further advancement, Yang *et al.* introduced a DNA circuit-based miRNA classifier, which enables arithmetic operations on localized DNA origami scaffolds for cancer diagnosis. This novel biosensor employs a 2D DNA origami as a framework to localize functional DNA strands as processing modules, facilitating localized strand displacement reactions for arithmetic operations such as multiplication, addition, and subtraction. These operations mimic the computational logic of a support vector machine, allowing the system to classify complex miRNA input patterns from patient samples with high precision. The result showed that the DNA classifier system can provide an accurate cancer diagnosis in about 3 hours, which is significantly faster and more effective than traditional, non-localized DNA circuits.

Moreover, the spatial addressability of DNA origami extends multiplexed sensing toward multivalent biosensing for improved cell recognition. Sun *et al.* created an origami-based design of peptide-major histocompatibility complex (pMHC) multimers for detecting low-affinity T cells.[112] The authors fabricated 2D triangular origami with biotinylated overhangs to introduce streptavidin (SA) molecules to the origami surfaces with nanoscale precision. Biotinylated pMHC molecules were then attached to SA sites on the origami templates, forming various origami-guided pMHC multimers with finely tuned spacing and valency. This multivalent presentation of pMHC significantly increased the binding avidity for antigen-specific T cell receptors (TCRs). Relatively shorter inter-pMHC spacing and higher pMHC valency showed greater binding efficacy. To identify autoimmune $CD8^{+}$ T cells from the spleen of nonobese diabetic (NOD) mice, these origami-based pMHC multimers outperformed in staining efficiency and background compared with dextramers with equivalent pMHC concentrations. This DNA origami platform enables fine-tuning of pMHC presentation for improved detection of elusive T cell populations, making it a powerful tool in studies of immune function and immunotherapy.

Inspired by immune synapse recognition, Mao *et al.* developed modular DNA origami-based aptamer nanoarrays for enhanced capture of circulating tumor cells (Fig. 4c).[113] Using 2D triangular DNA origamis as scaffolds, multiple copies of different aptamers for recognizing specific proteins expressed on tumor cells (such as epithelial cellular adhesion molecule, EpCAM; epidermal growth factor receptor, EGFR; and human epidermal growth factor receptor 2, HER2), were organized with nanoscale precision, forming modular arrays with multi-ligands. The valency and inter-molecule spacing of aptamers can be fine-tuned on the origami templates to topologically match the target protein clusters on the tumor cells. This design resulted in a significant enhancement in binding affinity, with one modular aptamer nanoarray showing a ~3000-fold increase compared to a monovalent aptamer. The design enabled the high-efficiency and unbiased capture of circulating tumor cells from clinical samples. This programmable nanoarray may provide a powerful new tool for high-affinity clinical detection and cell engineering.

Collectively, these examples demonstrate how DNA nanodevices progress from simultaneous detection of multiple targets to logic-based classification, and, finally, to multivalent recognition, offering powerful platforms for complex biosensing tasks.

4.3. Targeted molecular bioimaging

In parallel with detection applications, molecular bioimaging offers complementary advantages by providing spatial information about biomolecule distribution within cellular and tissue environments. This enables not only accurate diagnosis but also real-time monitoring of disease progression. DNA nanostructures are particularly attractive for such applications due to their preferential localization in subcellular compartments or specific organs, as well as their ability to be functionalized with targeting ligands for precise delivery.

At the subcellular level, Leung *et al.* engineered a DNA nanomachine for *in situ* detection of H^{+} and Cl^{-} in lysosomes (Fig. 5a).[114] The nanomachine was a DNA duplex with three modules: a Cl^{-}-sensing module containing a Cl^{-}-binding fluorophore; an H^{+}-sensing module containing an i-motif sequence; and a normalizing module with a Cl^{-}/H^{+}-insensitive fluorophore that served as an internal reference for ratiometric reporting of both ions. In acidic environments, the i-motif sequence underwent a conformational change and generated a FRET signal. This design facilitated the ratiometric and simultaneous analysis of pH and Cl^{-} within a single lysosome.

In a related approach, Yi *et al.* developed a DNAzyme-based sensing system for subcellular compartment-specific imaging of Zn^{2+}, which was based on the variations of ribosomal RNA (rRNA) across distinct subcellular regions.[115] The sensor

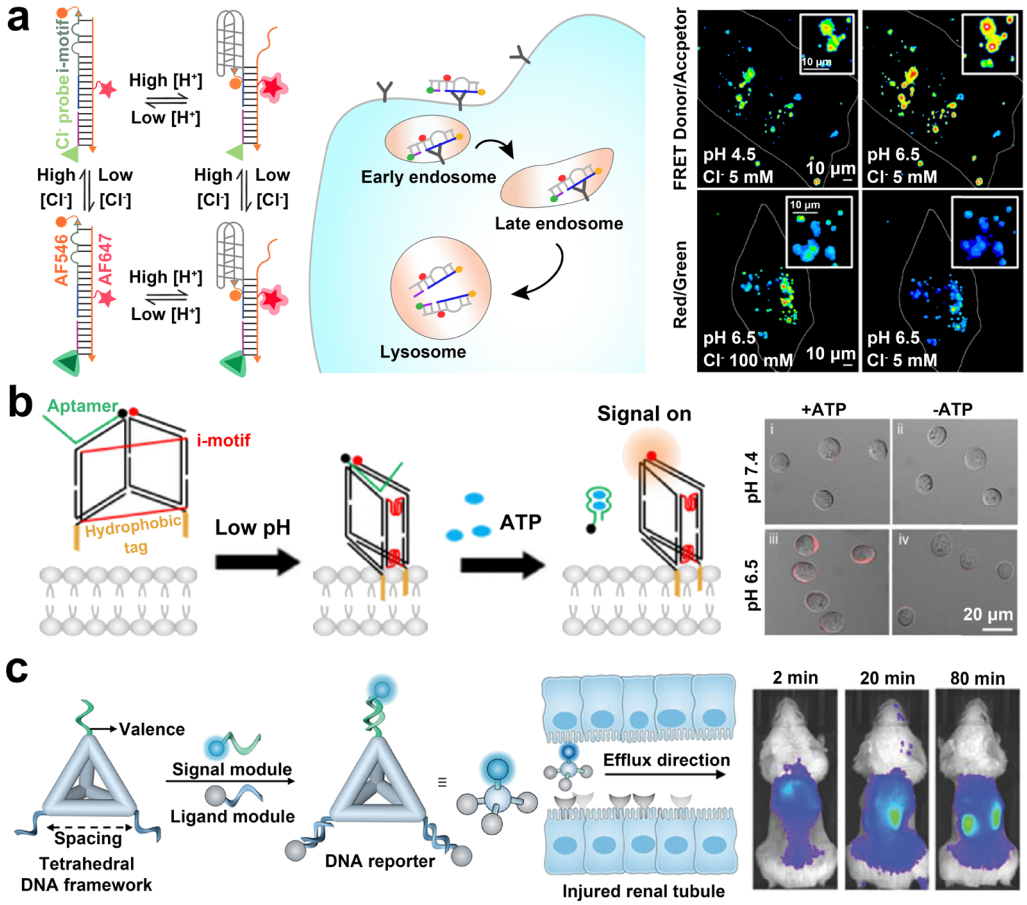

Fig. 5 Self-assembled DNA nanodevices for targeted molecular bioimaging. (a) DNA nanomachine for the detection of H^+ and Cl^-. Reproduced with permission from ref. 114. Copyright 2019, Spinger Nature. (b) DNA prism-based sensor for ATP imaging in tumor microenvironments. Reproduced with permission from ref. 116. Copyright 2025, John Wiley and Sons. (c) Tetrahedral DNA frameworks for protein biomarker sensing and kidney injury reporting. Reproduced with permission from ref. 120. Copyright 2024, John Wiley and Sons.

consisted of two elements: an rRNA-activatable DNAzyme sensing module and a MB-based signal amplification module. The Zn^{2+}-specific DNAzyme was initially blocked by hybridizing with a DNA sequence containing a toehold region, which could be specifically displaced by mitochondria-localized 12S rRNA or cytosolic 18S rRNA, thereby releasing the active DNAzyme. Upon encountering Zn^{2+}, the active DNAzyme cleaved the substrate MBs, leading to their stem breakage and fluorescence recovery. This system enabled the *in situ* monitoring of subcellular dynamics of mitochondrial Zn^{2+} during ischemia and the drug intervention.

Extending from the cellular scale, DNA-based nanosensors have been developed for targeted molecular imaging on tumor cell membrane. Li *et al.* presented a triangular DNA prism-based nanosensor for ATP imaging on tumor cell membranes (Fig. 5b).[116] This sensor incorporated palmitic acid anchors, i-motif sequences, and an ATP aptamer in a DNA prism structure. The i-motif sequences in the sensors dynamically reconfigured under acidic conditions of the TME (pH 6.5–6.8), bringing the hydrophobic palmitic acid tags closer together and enhancing membrane anchoring. After the DNA nanoprobe was specifically anchored onto the cell membrane, the BHQ2-tagged ATP aptamer could bind to ATP and detach from the DNA structure, restoring Cy5 fluorescence for tumor imaging.

For dynamic monitoring of therapeutic responses, Zheng *et al.* designed a membrane-attached DNA nanostructure for real-time detection of ATP efflux from apoptotic cancer cells.[117] DNA triangle frameworks were integrated with cholesterol for cell membrane attachment. These DNA frameworks tethered branched vertexes (3WJ and 4WJ) assembled as structural engineering components, in which G-quadruplexes and i-motifs were involved to form a heterodimeric folding triggered by TME biomarkers (both K^+ and H^+). Split ATP aptamers were also tagged onto the 3WJ-triangles and 4WJ-triangles. The presence of K^+ and H^+, promoted the heterodimeric dimerization of the 3WJ-triangles and 4WJ-triangles, bringing the two parts of the ATP aptamers into close proximity on the cell surface. When ATP molecules were released from the doxorubicin-treated, apoptotic cancer cells, they were interacted with the aptamer-displaying DNA frameworks, a process that was sensed by half-aptamer-tagged Cy3/Cy5 FRET pairs. This enabled real-time monitoring of drug-stimulated apoptosis by detecting ATP efflux, offering a sensitive, non-invasive approach for dynamically evaluating therapeutic efficacy.

At the organ level, DNA nanostructures have also demonstrated remarkable potential for organ-specific bioimaging. Zhao *et al.* developed a DNA origami-based platform for kidney-targeted miRNA sensing in acute kidney injury (AKI) models.[118] The DNA origami was constructed and modified with Cy5-tagged strands, which were initially quenched by BHQ3-tagged ssDNA strands. When encountering elevated levels of the biomarker miR-21 during AKI,[119] a strand displacement reaction was triggered, releasing BHQ3-tagged strands and restoring the fluorescence signal for real-time detection. In addition, the photoacoustic changes from BHQ3, owing to the varied excretion rates between the nanostructure and released BHQ3-labeled DNA strands, enabled dual-mode imaging for enhanced diagnostic accuracy.

In another example, Ding *et al.* designed tetrahedral DNA framework (TDF)-based sensors for detecting Kim-1 protein (Fig. 5c),[120] a biomarker of kidney injury that is highly expressed by damaged renal proximal tubular cells.[121] They designed three TDFs with different edge lengths (5.8 nm, 12.6 nm, and 36 nm), and used these TDFs as connecting cores to precisely control the valency and spacing of the peptide ligands. Through the interaction with damaged, Kim-1-positive renal tubular epithelial cells with these peptide-TDFs, *in vivo* testing and urinalysis for glycerol-induced AKI mice were achieved, with Cy7 employed as the signal module. The TDF sensors with an edge length of 5.8 nm and three attached ligands showed significant kidney fluorescence in AKI mice compared to healthy mice. These injected sensors can also detect Kim-1 signals in urine samples collected at different time points after AKI onset, demonstrating the potential for precise urinalysis of disease-associated membrane protein markers. These advances, spanning from subcellular imaging to organ-level diagnostics, illustrate the broad adaptability of self-assembled DNA nanodevices for targeted molecular bioimaging in different levels of biomedical diagnosis.

Taken together, the recent advancements in self-assembled DNA nanodevices highlight their potential for next-generation biosensing. Ultrasensitive detection strategies push the analytical limits by enabling reliable identification of trace biomolecules, while multiplexed sensing expands diagnostic capability to accommodate the complexity of real-world biological systems. Complementarily, targeted molecular bioimaging provides spatial and temporal resolution, allowing the visualization of molecular events within relevant cellular or tissue contexts. These three aspects are synergistic and collectively pave the way toward highly integrated, multifunctional, and intelligent biosensing systems.

5. Summary and perspectives

Structural DNA nanotechnology has emerged as a powerful tool for the construction of artificial architectures with precise geometries and versatile functions. This minireview highlights how these self-assembled DNA nanodevices have been designed and engineered for the efficient and intelligent sensing of various molecular targets. Remarkable advances have been made in the design of diverse DNA-based assemblies, such as DNA strands, multi-arm junction frameworks, and origami structures, which serve as scaffolds to organize sensing and signal-reporting modules for the construction of biosensors.

These sensors employ a variety of attractive ligands, such as aptamers, antibodies, DNAzymes, and i-motifs, to specifically recognize chemical or biological analytes. Upon binding to the targets, these biosensors are programmed to generate diverse reporting signals, including fluorescence, electronic signals, plasmonic CD, and single-molecule SERS. These advances offer innovative solutions for biomedical diagnostics and environmental surveillance. The design and application of these self-assembled DNA nanodevices for biosensing therefore represent a significant technological step forward, offering exceptional programmability and specificity for molecular detection.

While highly promising, DNA nanodevice-based biosensors face several critical challenges that must be overcome to bridge the gap between their current laboratory performance and future clinical practice.

5.1. Detection precision and capabilities

To meet the demands of advanced applications, such as early-stage cancer diagnosis, DNA nanotechnology must evolve toward more sophisticated smart sensors capable of executing complex sensing and reporting actions. The challenge is that cancers are highly heterogeneous and continuously mutating, and many single oncogenic targets overlap with normal tissues, compromising precision. Thus, future intelligent sensors must be able to interact with multi-component systems and decipher multifaceted signal patterns arising from intact tumor cells and their microenvironments. In principle, improved cancer sensing precision can be achieved by recognizing multiple targets or even patterns of molecular features, instead of focusing on single molecules alone.

To address this demand, DNA nanodevices can be engineered to integrate different sensing ligands within distinct structural modules, enabling the simultaneous detection of multiple targets.[122,123] Designing nanodevices with multivalent ligand arrangements in precise spatial patterns can further enhance binding specificity through cooperative interactions.[124,125] Recent work on DNA logic circuits incorporating AND/NOT gates has demonstrated that these devices can discriminate malignant cells from normal tissues with high precision.[126–130] These strategies highlight the promise of logic-gated sensing and molecular computation for future intelligent biosensor design.

Another significant challenge is the reliable detection of low-abundance signals in complex biological environments. Signal amplification strategies, such as isothermal enzymatic reactions and hairpin-based self-assembly, have already shown promise for amplifying trace signals.[49,131,132] Beyond these nucleic acid-based amplification, diverse signal amplification modules can be integrated into DNA nanodevice-based biosensing platforms, including fluorescence-quencher beacons, plasmonic nanoparticles, field-effect transistors, photonic crystal

devices, and noble metal electrodes, which will enhance detection reliability and sensitivity for early-stage disease diagnosis.

For future diagnostic applications requiring *in vivo* real-time imaging, challenges remain with tissue penetration and biofluid complexity, which often limit sensor performance. Addressing these issues may involve designing sensors that perform multi-tiered reporting actions or incorporating advanced imaging elements, such as chemiluminescence probes, NIR-II dyes, and quantum dots. These improvements would help minimize tissue autofluorescence, increase penetration depth, and improve signal-to-background ratios. Looking further ahead, combining intelligent DNA sensors with machine learning could enable predictive and adaptive biosensor design, ultimately supporting personalized diagnostics.[133–135]

5.2. Pharmacokinetic studies

For *in vivo* applications, finely tuned pharmacokinetic properties are critical. Distinct sensing tasks require specific biodistribution and clearance profiles. For example, sensors for early cancer diagnosis and tumor imaging often benefit from prolonged circulation times, which improve passive tumor accumulation. Conversely, fast kidney clearance is advantageous for acute kidney injury detection and urinalysis. Thus, different applications necessitate a tailored balance between circulation half-life and clearance rates.

Future DNA-based biosensors could be designed as pharmacokinetically switchable systems. Such sensors could accumulate at disease sites for localized analysis, followed by rapid clearance for biofluid-based readouts. Achieving these pharmacokinetic properties will require precise regulation of structural features such as size, charge, and ligand density. More advanced multifunctional systems could be built by conjugating long-circulating elements with rapidly excreted modules *via* biomarker-responsive linkers, enabling site-specific activation followed by controlled excretion.

5.3. Stability, safety and mass production

Another set of challenges for DNA-based biosensors involves their stability, biocompatibility, and large-scale manufacturing. DNA strands are highly susceptible to enzymatic degradation by nucleases present in biological fluids such as blood and urine. The performance of DNA-based biosensors is also compromised by environmental factors, including temperature and ion concentration fluctuations. Moreover, repeated use of DNA biosensors may result in the denaturation of biomolecular probes, reducing their sensing capabilities over multiple cycles.[136]

The most common approaches to enhance the stability of nucleic acid strands are chemical modifications such as phosphorothioate linkages and 2′-O-methyl ribose modifications. These unnatural analogues, already used in clinically approved nucleic acid drugs,[137] can increase the resistance of DNA nanodevices to enzymatic degradation, thereby prolonging their lifespan. Additionally, protective coating with block polymers such as PEG or PEGylated oligolysine has been demonstrated to enhance the structural integrity and extend the half-life of DNA materials in blood circulation.[138,139] This highlights the polymer coating strategy to increase the stability of DNA-based nanodevices in a biological environment. While chemical modifications and protective coatings can enhance structural stability and extend the operational lifetime of these nanodevices, such alterations may come at the cost of reduced sensitivity to target molecules.

Safety is equally crucial for clinical applications. Encouragingly, recent work has shown that endotoxin removal during scaffold DNA preparation can significantly reduce immune responses, suggesting that DNA origami can serve as a safe biosensing platform.[140] DNA nanotechnology has also enabled precise immunomodulation by assembling antigens or adjuvants with nanoscale precision on the DNA origami surfaces.[141,142] Finally, the mass production of DNA-based materials is currently challenging due to the high cost of synthesizing modified oligonucleotide conjugates. Scaling up the precise self-assembly processes from a laboratory to an industrial setting presents considerable technical hurdles.

In summary, self-assembled DNA nanodevices offer unique programmability, specificity, and modularity, which make them powerful candidates for next-generation biosensing. To achieve clinical translation, future research should focus on these key areas: (1) integrating multiplexed sensing, amplifying, and imaging functions into unified nanodevices for comprehensive profiling; (2) enhancing pharmacokinetic tunability, stability, and safety for *in vivo* applications; and (3) developing cost-effective and scalable manufacturing pipelines. Combining DNA-based biosensing with artificial intelligence and machine learning has particular promise for accelerating data interpretation and guiding sensor design. Overall, structural DNA nanotechnology stands at the frontier of biosensing innovation. With continued development, it has the potential to transform both fundamental biological research and clinical diagnostics, paving the way for precision medicine and real-time disease monitoring.

Author contributions

Y. C. and R. T. contributed equally to this work. Y. C. and R. T.: conceptualization, writing – original draft, visualization, writing – review & editing. Y. Z.: writing – review & editing. B. D. and Q. J.: supervision, conceptualization, writing – original draft, writing – review & editing, funding acquisition.

Conflicts of interest

There are no conflicts to declare.

Data availability

This is a review article, and all the referred data and schematics have been previously published. The schematics and illustrations are available upon request.

Acknowledgements

This work is supported by the National Natural Science Foundation of China (grant no. 22322702, 22025201, 32071389, and 22107022), the National Key R&D Program of China National Basic Research Program of China (grant no. 2021YFA1200302 and 2021YFA1201201), the Strategic Priority Research Program of Chinese Academy of Sciences (grant no. XDB36000000), the Youth Innovation Promotion Association, Chinese Academy of Sciences (CAS), the CAS Interdisciplinary Innovation Team, the K.C. Wong Education Foundation (grant no. GJTD-2018-03), and the CAS Project for Young Scientists in Basic Research (grant no. YSBR-036).

References

1 A. D. Hershey and M. Chase, *J. Gen. Physiol.*, 1952, **36**, 39–56.
2 J. D. Watson and F. H. Crick, *Nature*, 1953, **171**, 737–738.
3 N. C. Seeman, *J. Theor. Biol.*, 1982, **99**, 237–247.
4 X. Wang and N. C. Seeman, *J. Am. Chem. Soc.*, 2007, **129**, 8169–8176.
5 H. Yan, S. H. Park, G. Finkelstein, J. H. Reif and T. H. LaBean, *Science*, 2003, **301**, 1882–1884.
6 R. P. Goodman, I. A. Schaap, C. F. Tardin, C. M. Erben, R. M. Berry, C. F. Schmidt and A. J. Turberfield, *Science*, 2005, **310**, 1661–1665.
7 Y. He, T. Ye, M. Su, C. Zhang, A. E. Ribbe, W. Jiang, C. Mao, Y. He, T. Ye, M. Su, C. Zhang, A. E. Ribbe, W. Jiang and C. Mao, *Nature*, 2008, **452**, 198–201.
8 J. Zheng, J. J. Birktoft, Y. Chen, T. Wang, R. Sha, P. E. Constantinou, S. L. Ginell, C. Mao, N. C. Seeman, J. Zheng, J. J. Birktoft, Y. Chen, T. Wang, R. Sha, P. E. Constantinou, S. L. Ginell, C. Mao and N. C. Seeman, *Nature*, 2009, **461**, 74–77.
9 P. W. Rothemund, *Nature*, 2006, **440**, 297–302.
10 Y. Ke, S. Lindsay, Y. Chang, Y. Liu and H. Yan, *Science*, 2008, **319**, 180–183.
11 R. J. Kershner, L. D. Bozano, C. M. Micheel, A. M. Hung, A. R. Fornof, J. N. Cha, C. T. Rettner, M. Bersani, J. Frommer, P. W. Rothemund and G. M. Wallraff, *Nat. Nanotechnol.*, 2009, **4**, 557–561.
12 G. Tikhomirov, P. Petersen and L. Qian, *Nature*, 2017, **552**, 67–71.
13 Y. Wang, H. Wang, Y. Li, C. Yang, Y. Tang, X. Lu, J. Fan, W. Tang, Y. Shang, H. Yan, J. Liu and B. Ding, *J. Am. Chem. Soc.*, 2024, **146**, 4178–4186.
14 S. M. Douglas, H. Dietz, T. Liedl, B. Hogberg, F. Graf and W. M. Shih, *Nature*, 2009, **459**, 414–418.
15 D. Han, S. Pal, Y. Liu and H. Yan, *Nat. Nanotechnol.*, 2010, **5**, 712–717.
16 T. Liedl, B. Hogberg, J. Tytell, D. E. Ingber and W. M. Shih, *Nat. Nanotechnol.*, 2010, **5**, 520–524.
17 D. Han, S. Pal, J. Nangreave, Z. Deng, Y. Liu and H. Yan, *Science*, 2011, **332**, 342–346.
18 E. S. Andersen, M. Dong, M. M. Nielsen, K. Jahn, R. Subramani, W. Mamdouh, M. M. Golas, B. Sander, H. Stark, C. L. P. Oliveira, J. S. Pedersen, V. Birkedal, F. Besenbacher, K. V. Gothelf, J. Kjems, E. S. Andersen, M. Dong, M. M. Nielsen, K. Jahn, R. Subramani, W. Mamdouh, M. M. Golas, B. Sander, H. Stark, C. L. P. Oliveira, J. S. Pedersen, V. Birkedal, F. Besenbacher, K. V. Gothelf and J. Kjems, *Nature*, 2009, **459**, 73–76.
19 J. J. Funke and H. Dietz, *Nat. Nanotechnol.*, 2016, **11**, 47–52.
20 J. Schnitzbauer, M. T. Strauss, T. Schlichthaerle, F. Schueder, R. Jungmann, J. Schnitzbauer, M. T. Strauss, T. Schlichthaerle, F. Schueder and R. Jungmann, *Nat. Protoc.*, 2017, **12**, 1198–1228.
21 Y. Wang, I. Baars, F. Fördös and B. Högberg, *ACS Nano*, 2021, **15**, 9614–9626.
22 S. Zhao, R. Tian, J. Wu, S. Liu, Y. Wang, M. Wen, Y. Shang, Q. Liu, Y. Li, Y. Guo, Z. Wang, T. Wang, Y. Zhao, H. Zhao, H. Cao, Y. Su, J. Sun, Q. Jiang, B. Ding, S. Zhao, R. Tian, J. Wu, S. Liu, Y. Wang, M. Wen, Y. Shang, Q. Liu, Y. Li, Y. Guo, Z. Wang, T. Wang, Y. Zhao, H. Zhao, H. Cao, Y. Su, J. Sun, Q. Jiang and B. Ding, *Nat. Commun.*, 2021, **12**, 358.
23 N. Sarraf, K. R. Rodriguez and L. Qian, *Sci. Rob.*, 2023, **8**, eadf1511.
24 E.-M. Roller, L. V. Besteiro, C. Pupp, L. K. Khorashad, A. O. Govorov, T. Liedl, E.-M. Roller, L. V. Besteiro, C. Pupp, L. K. Khorashad, A. O. Govorov and T. Liedl, *Nat. Phys.*, 2017, **13**, 761–765.
25 P. Zhan, T. Wen, Z. G. Wang, Y. He, J. Shi, T. Wang, X. Liu, G. Lu and B. Ding, *Angew. Chem., Int. Ed.*, 2018, **57**, 2846–2850.
26 Y. Shang, N. Li, S. Liu, L. Wang, Z. G. Wang, Z. Zhang and B. Ding, *Adv. Mater.*, 2020, **32**, e2000294.
27 H. Lv, N. Xie, M. Li, M. Dong, C. Sun, Q. Zhang, L. Zhao, J. Li, X. Zuo, H. Chen, F. Wang, C. Fan, H. Lv, N. Xie, M. Li, M. Dong, C. Sun, Q. Zhang, L. Zhao, J. Li, X. Zuo, H. Chen, F. Wang and C. Fan, *Nature*, 2023, **622**, 292–300.
28 A.-K. Pumm, W. Engelen, E. Kopperger, J. Isensee, M. Vogt, V. Kozina, M. Kube, M. N. Honemann, E. Bertosin, M. Langecker, R. Golestanian, F. C. Simmel, H. Dietz, A.-K. Pumm, W. Engelen, E. Kopperger, J. Isensee, M. Vogt, V. Kozina, M. Kube, M. N. Honemann, E. Bertosin, M. Langecker, R. Golestanian, F. C. Simmel and H. Dietz, *Nature*, 2022, **607**, 492–498.
29 T. Gerling, K. F. Wagenbauer, A. M. Neuner and H. Dietz, *Science*, 2015, **347**, 1446–1452.
30 A. E. Marras, L. Zhou, H.-J. Su, C. E. Castro, A. E. Marras, L. Zhou, H.-J. Su and C. E. Castro, *Proc. Natl. Acad. Sci. U. S. A.*, 2015, **112**, 713–718.
31 S. M. Douglas, I. Bachelet and G. M. Church, *Science*, 2012, **335**, 831–834.
32 S. Li, Q. Jiang, S. Liu, Y. Zhang, Y. Tian, C. Song, J. Wang, Y. Zou, G. J. Anderson, J. Y. Han, Y. Chang, Y. Liu, C. Zhang, L. Chen, G. Zhou, G. Nie, H. Yan, B. Ding and Y. Zhao, *Nat. Biotechnol.*, 2018, **36**, 258–264.
33 Z. Wang, L. Song, Q. Liu, R. Tian, Y. Shang, F. Liu, S. Liu, S. Zhao, Z. Han, J. Sun, Q. Jiang and B. Ding, *Angew. Chem., Int. Ed.*, 2021, **60**, 2594–2598.

34 S. Liu, Q. Jiang, X. Zhao, R. Zhao, Y. Wang, Y. Wang, J. Liu, Y. Shang, S. Zhao, T. Wu, Y. Zhang, G. Nie and B. Ding, *Nat. Mater.*, 2021, **20**, 421–430.
35 J. Yin, S. Wang, J. Wang, Y. Zhang, C. Fan, J. Chao, Y. Gao, L. Wang, J. Yin, S. Wang, J. Wang, Y. Zhang, C. Fan, J. Chao, Y. Gao and L. Wang, *Nat. Mater.*, 2024, **23**, 854–862.
36 Y. Wang, I. Baars, I. Berzina, I. Rocamonde-Lago, B. Shen, Y. Yang, M. Lolaico, J. Waldvogel, I. Smyrlaki, K. Zhu, R. A. Harris, B. Högberg, Y. Wang, I. Baars, I. Berzina, I. Rocamonde-Lago, B. Shen, Y. Yang, M. Lolaico, J. Waldvogel, I. Smyrlaki, K. Zhu, R. A. Harris and B. Högberg, *Nat. Nanotechnol.*, 2024, **19**, 1366–1374.
37 L. Zhao, F. Ahmed, Y. Zeng, W. Xu and H. Xiong, *ACS Sens.*, 2022, **7**, 2833–2856.
38 M. Debnath, K. Fatma and J. Dash, *Angew. Chem., Int. Ed.*, 2019, **58**, 2942.
39 L. Wu, Y. Wang, X. Xu, Y. Liu, B. Lin, M. Zhang, J. Zhang, S. Wan, C. Yang and W. Tan, *Chem. Rev.*, 2021, **121**, 12035–12105.
40 X. B. Zhang, R. M. Kong and Y. Lu, *Annu. Rev. Anal. Chem.*, 2011, **4**, 105–128.
41 J. Su, C. Sun, J. Du, X. Xing, F. Wang and H. Dong, *Adv. Healthcare Mater.*, 2023, **12**, 2300367.
42 C. Lodeiro, J. L. Capelo, J. C. Mejuto, E. Oliveira, H. M. Santos, B. Pedras and C. Nuñez, *Chem. Soc. Rev.*, 2010, **39**, 2948–2976.
43 Q. Liu, J. Wang and B. J. Boyd, *Talanta*, 2015, **136**, 114–127.
44 A. Gangar, A. Fegan, S. C. Kumarapperuma and C. R. Wagner, *J. Am. Chem. Soc.*, 2012, **134**, 2895–2897.
45 L. Wang, Y. Sang, M. Hu, Y. Bao, N. Wang, X. Yan and Y. Dong, *Microchem. J.*, 2025, **208**, 112351.
46 W. E. Briley, M. H. Bondy, P. S. Randeria, T. J. Dupper, C. A. Mirkin, W. E. Briley, M. H. Bondy, P. S. Randeria, T. J. Dupper and C. A. Mirkin, *Proc. Natl. Acad. Sci. U. S. A.*, 2015, **112**, 9591–9595.
47 M. M. Ali, F. Li, Z. Zhang, K. Zhang, D.-K. Kang, J. A. Ankrum, X. C. Le and W. Zhao, *Chem. Soc. Rev.*, 2014, **43**, 3324–3341.
48 S. Bi, S. Yue and S. Zhang, *Chem. Soc. Rev.*, 2017, **46**, 4281–4298.
49 F. Wang, C.-H. Lu and I. Willner, *Chem. Rev.*, 2014, **114**, 2881–2941.
50 L. Shi, Y. Liu, X. Li, H. Zhang, Z. Wang, S. He, D. Fan, X. Huang, Y. Zi, Y. Han, D. Zhang and X. Chen, *ACS Sens.*, 2025, **10**, 1579–1599.
51 S. Wu, H. Xia, J. Xu, X. Sun and X. Liu, *Adv. Mater.*, 2018, **30**, 1803362.
52 M. F. Perutz, *Annu. Rev. Biochem.*, 1979, **48**, 327–386.
53 K. J. Swartz, *Nature*, 2008, **456**, 891–897.
54 A. Chacinska, C. M. Koehler, D. Milenkovic, T. Lithgow and N. Pfanner, *Cell*, 2009, **138**, 628–644.
55 J. S. Hleap, E. Susko, C. Blouin, J. S. Hleap, E. Susko and C. Blouin, *BMC Struct. Biol.*, 2013, **13**, 20.
56 E. Lloyd-Evans, A. J. Morgan, X. He, D. A. Smith, E. Elliot-Smith, D. J. Sillence, G. C. Churchill, E. H. Schuchman, A. Galione, F. M. Platt, E. Lloyd-Evans, A. J. Morgan, X. He, D. A. Smith, E. Elliot-Smith, D. J. Sillence, G. C. Churchill, E. H. Schuchman, A. Galione and F. M. Platt, *Nat. Med.*, 2008, **14**, 1247–1255.
57 J. P. Luzio, P. R. Pryor, N. A. Bright, J. P. Luzio, P. R. Pryor and N. A. Bright, *Nat. Rev. Mol. Cell Biol.*, 2007, **8**, 622–632.
58 G. Y. Zou, F. Bi, Y. L. Yu, M. X. Liu and S. Chen, *Anal. Chem.*, 2024, **96**, 16639–16648.
59 X. Yue, Y. Qiao, D. Gu, R. Qi, H. Zhao, Y. Yin, W. Zhao, R. Xi and M. Meng, *Anal. Chem.*, 2021, **93**, 7250–7257.
60 C. Cang, B. Bekele, D. Ren, C. Cang, B. Bekele and D. Ren, *Nat. Chem. Biol.*, 2014, **10**, 463–469.
61 B. Foo, B. Williamson, J. C. Young, G. Lukacs and A. Shrier, *J. Physiol.-London*, 2016, **594**, 2469–2481.
62 J. Zou, K. Mitra, P. Anees, D. Oettinger, J. R. Ramirez, A. T. Veetil, P. D. Gupta, R. Rao, J. J. Smith, P. Kratsios and Y. Krishnan, *Nat. Biotechnol.*, 2024, **42**, 1075–1083.
63 J. H. Kaplan, *Annu. Rev. Biochem.*, 2002, **71**, 511–535.
64 P. Anees, A. Saminathan, E. R. Rozmus, A. Di, A. B. Malik, B. P. Delisle and Y. Krishnan, *Nat. Biotechnol.*, 2024, **42**, 1065–1074.
65 S. L. Sensi, P. Paoletti, A. I. Bush, I. Sekler, S. L. Sensi, P. Paoletti, A. I. Bush and I. Sekler, *Nat. Rev. Neurosci.*, 2009, **10**, 780–791.
66 X. Wang, G. Kim, J. L. Chu, T. Song, Z. Yang, W. Guo, X. Shao, M. L. Oelze, K. C. Li and Y. Lu, *J. Am. Chem. Soc.*, 2022, **144**, 5812–5819.
67 K. Jomova, S. Y. Alomar, E. Nepovimova, K. Kuca, M. Valko, K. Jomova, S. Y. Alomar, E. Nepovimova, K. Kuca and M. Valko, *Arch. Toxicol.*, 2024, **99**, 153–209.
68 N. B. Abramenko, T. B. Demidova, V. Abkhalimov, B. G. Ershov, E. Y. Krysanov and L. M. Kustov, *J. Hazard. Mater.*, 2018, **347**, 89–94.
69 X. Qu, F. Yang, H. Chen, J. Li, H. Zhang, G. Zhang, L. Li, L. Wang, S. Song, Y. Tian and H. Pei, *ACS Appl. Mater. Interfaces*, 2017, **9**, 16026–16034.
70 C. Reily, T. J. Stewart, M. B. Renfrow, J. Novak, C. Reily, T. J. Stewart, M. B. Renfrow and J. Novak, *Nat. Rev. Nephrol.*, 2019, **15**, 346–366.
71 M. Yoshida, E. Muneyuki, T. Hisabori, M. Yoshida, E. Muneyuki and T. Hisabori, *Nat. Rev. Mol. Cell Biol.*, 2001, **2**, 669–677.
72 C. Puchades, C. R. Sandate, G. C. Lander, C. Puchades, C. R. Sandate and G. C. Lander, *Nat. Rev. Mol. Cell Biol.*, 2019, **21**, 43–58.
73 F. Di Virgilio, A. C. Sarti, S. Falzoni, E. De Marchi, E. Adinolfi, F. Di Virgilio, A. C. Sarti, S. Falzoni, E. De Marchi and E. Adinolfi, *Nat. Rev. Cancer*, 2018, **18**, 601–618.
74 P. Pellegatti, L. Raffaghello, G. Bianchi, F. Piccardi, V. Pistoia and F. D. Virgilio, *PLOS ONE*, 2008, **3**, e2599.
75 S. Thakkar, D. Sharma, K. Kalia and R. K. Tekade, *Acta Biomater.*, 2020, **101**, 43–68.
76 L. Ai, Q. Zuo, Y. Li, S. Wu, Y. Sima, Y. Zhang, S. Xie, Z. Zhao and W. Tan, *ACS Nano*, 2023, **17**, 13430–13440.
77 X. Cheng, H.-D. Xu, H.-H. Ran, G. Liang and F.-G. Wu, *ACS Nano*, 2021, **15**, 8039–8068.

78 X. Chai, Z. Fan, M. M. Yu, J. Zhao and L. Li, *Nano Lett.*, 2021, **21**, 10047–10053.
79 X. Li, X. Xu, K. Wang, Y. Chen, Y. Zhang, Q. Si, Z. Pan, F. Jia, X. Cui, X. Wang, X. Deng, Y. Zhao, D. Shu, Q. Jiang, B. Ding, Y. Wu and R. Liu, *Adv. Mater.*, 2023, **35**, e2208820.
80 S. Chen, T. L. Liu, Y. Dong and J. Li, *ACS Nano*, 2022, **16**, 20922–20936.
81 L. Wang, X. Wang, Y. Wu, M. Guo, C. Gu, C. Dai, D. Kong, Y. Wang, C. Zhang, D. Qu, C. Fan, Y. Xie, Z. Zhu, Y. Liu and D. Wei, *Nat. Biomed. Eng.*, 2022, **6**, 276–285.
82 R. Shang, S. Lee, G. Senavirathne, E. C. Lai, R. Shang, S. Lee, G. Senavirathne and E. C. Lai, *Nat. Rev. Genet.*, 2023, **24**, 816–833.
83 G. A. Calin, C. M. Croce, G. A. Calin and C. M. Croce, *Nat. Rev. Cancer*, 2006, **6**, 857–866.
84 S. Zhao, S. Zhang, H. Hu, Y. Cheng, K. Zou, J. Song, J. Deng, L. Li, X. B. Zhang, G. Ke and J. Sun, *Angew. Chem., Int. Ed.*, 2023, **62**, e202303121.
85 Z. Zhou, N. Lin, Y. Ouyang, S. Liu, Y. Zhang and I. Willner, *J. Am. Chem. Soc.*, 2023, **145**, 12617–12629.
86 Y. Liu, A. Beyer and R. Aebersold, *Cell*, 2016, **165**, 535–550.
87 W. Ma, B. Chen, R. Jia, H. Sun, J. Huang, H. Cheng, H. Wang, X. He and K. Wang, *Anal. Chem.*, 2021, **93**, 10511–10518.
88 Y. Zhou, L. Tao, J. Qiu, J. Xu, X. Yang, Y. Zhang, X. Tian, X. Guan, X. Cen, Y. Zhao, Y. Zhou, L. Tao, J. Qiu, J. Xu, X. Yang, Y. Zhang, X. Tian, X. Guan, X. Cen and Y. Zhao, *Signal Transduct. Target. Ther.*, 2024, **9**, 132.
89 M. A. Brown, Z. Li, K.-A. L. Cao, M. A. Brown, Z. Li and K.-A. L. Cao, *Nat. Rev. Rheumatol.*, 2020, **16**, 448–463.
90 E. MacLean, T. Broger, S. Yerlikaya, B. L. Fernandez-Carballo, M. Pai, C. M. Denkinger, E. MacLean, T. Broger, S. Yerlikaya, B. L. Fernandez-Carballo, M. Pai and C. M. Denkinger, *Nat. Microbiol.*, 2019, **4**, 748–758.
91 C.-M.-O. B. A. C. Consortium, *Cell*, 2022, **185**, 916–938.
92 Q. Zhao, D. Lu, G. Zhang, D. Zhang and X. Shi, *Talanta*, 2021, **223**, 121722.
93 R. Ayoubi, J. Ryan, S. Gonzalez Bolivar, C. Alende, V. Ruiz Moleon, M. Fotouhi, M. Alqazzaz, K. Southern, W. Alshafie, M. R. Baker, A. R. Ball, D. Callahan, J. A. Cooper, K. Crosby, K. J. Harvey, D. W. Houston, R. Kumaran, M. Rego, C. Schofield, H. Wu, M. S. Biddle, C. M. Brown, R. A. Kahn, A. Bandrowski, H. S. Virk, A. M. Edwards, P. S. McPherson, C. Laflamme, R. Ayoubi, J. Ryan, S. Gonzalez Bolivar, C. Alende, V. Ruiz Moleon, M. Fotouhi, M. Alqazzaz, K. Southern, W. Alshafie, M. R. Baker, A. R. Ball, D. Callahan, J. A. Cooper, K. Crosby, K. J. Harvey, D. W. Houston, R. Kumaran, M. Rego, C. Schofield, H. Wu, M. S. Biddle, C. M. Brown, R. A. Kahn, A. Bandrowski, H. S. Virk, A. M. Edwards, P. S. McPherson and C. Laflamme, *Nat. Protoc.*, 2024, **20**, 1509–1545.
94 H. Im, H. Shao, Y. I. Park, V. M. Peterson, C. M. Castro, R. Weissleder, H. Lee, H. Im, H. Shao, Y. I. Park, V. M. Peterson, C. M. Castro, R. Weissleder and H. Lee, *Nat. Biotechnol.*, 2014, **32**, 490–495.
95 N. Chauhan, Y. Xiong, S. Ren, A. Dwivedy, N. Magazine, L. Zhou, X. Jin, T. Zhang, B. T. Cunningham, S. Yao, W. Huang and X. Wang, *J. Am. Chem. Soc.*, 2023, **145**, 20214–20228.
96 L. Zhou, Y. Xiong, A. Dwivedy, M. Zheng, L. Cooper, S. Shepherd, T. Song, W. Hong, L. T. P. Le, X. Chen, S. Umrao, L. Rong, T. Wang, B. T. Cunningham and X. Wang, *Sci. Rob.*, 2024, **9**, eadi2084.
97 H. Ijäs, J. Trommler, L. Nguyen, S. van Rest, P. C. Nickels, T. Liedl and M. J. Urban, *Nat. Commun.*, 2025, **16**, 3216.
98 S. Chen, Z. Xu, S. Li, H. Liang, C. Zhang, Z. Wang, J. Li, J. Li and H. Yang, *Angew. Chem., Int. Ed.*, 2022, **61**, e202113795.
99 X. M. Zhou, S. Y. Chen, Y. Q. Chai, Y. Zhuo and R. Yuan, *Anal. Chem.*, 2025, **97**, 686–693.
100 B. Jia, J. Ge, Y. Ma, X. Sun, Z. Li, S. Jiang and H. Yu, *Angew. Chem., Int. Ed.*, 2024, **64**, e202421022.
101 Q. Ren, L. Jiang, S. Ma, T. Li, Y. Zhu, R. Qiu, Y. Xing, F. Yin, Z. Li, X. Ye, Y. Zhang and M. Zhang, *Adv. Mater.*, 2023, **35**, e2304119.
102 F. Liu, N. Li, Y. Shang, Y. Wang, Q. Liu, Z. Ma, Q. Jiang and B. Ding, *Angew. Chem., Int. Ed.*, 2022, **61**, e202114706.
103 A. Kuzyk, R. Schreiber, Z. Fan, G. Pardatscher, E. M. Roller, A. Hogele, F. C. Simmel, A. O. Govorov and T. Liedl, *Nature*, 2012, **483**, 311–314.
104 T. A. Feagin, D. P. Olsen, Z. C. Headman and J. M. Heemstra, *J. Am. Chem. Soc.*, 2015, **137**, 4198–4206.
105 F. Schuknecht, K. Kolataj, M. Steinberger, T. Liedl and T. Lohmueller, *Nat. Commun.*, 2023, **14**, 7192.
106 L. Grabenhorst, M. Pfeiffer, T. Schinkel, M. Kummerlin, G. A. Bruggenthies, J. B. Maglic, F. Selbach, A. T. Murr, P. Tinnefeld and V. Glembockyte, *Nat. Nanotechnol.*, 2025, **20**, 303–310.
107 J. Schnitzbauer, M. T. Strauss, T. Schlichthaerle, F. Schueder and R. Jungmann, *Nat. Protoc.*, 2017, **12**, 1198–1228.
108 C. Sun, K. Desch, B. Nassim-Assir, S. L. Giandomenico, P. Nemcova, J. D. Langer and E. M. Schuman, *Science*, 2023, **380**, eadf2018.
109 F. Bošković, J. Zhu, R. Tivony, A. Ohmann, K. Chen, M. F. Alawami, M. Dordevic, N. Ermann, J. Pereira-Dias, M. Fairhead, M. Howarth, S. Baker and U. F. Keyser, *Nat. Nanotechnol.*, 2023, **18**, 290–298.
110 R. Pavadai, A. Amalraj, S. Subramanian and P. Perumal, *ACS Appl. Mater. Interfaces*, 2021, **13**, 31710–31724.
111 T. Tu, S. Huan, X. Feng, G. Ke, L. Li and X. B. Zhang, *Angew. Chem., Int. Ed.*, 2025, **64**, e202424684.
112 Y. Sun, L. Yan, J. Sun, M. Xiao, W. Lai, G. Song, L. Li, C. Fan and H. Pei, *Nat. Commun.*, 2022, **13**, 3916.
113 M. Mao, Z. Lin, L. Chen, Z. Zou, J. Zhang, Q. Dou, J. Wu, J. Chen, M. Wu, L. Niu, C. Fan and Y. Zhang, *J. Am. Chem. Soc.*, 2023, **145**, 5447–5455.
114 K. Leung, K. Chakraborty, A. Saminathan and Y. Krishnan, *Nat. Nanotechnol.*, 2019, **14**, 176–183.
115 D. Yi, L. Li and M. Li, *Angew. Chem., Int. Ed.*, 2025, **64**, e202412387.
116 Q. Li, L. Wang, W. Xie, Q. Tan, S. Zhou, H. Pei, H. Zhang, J. Li, F. Qu and W. Tan, *Angew. Chem., Int. Ed.*, 2025, **64**, e202505223.

117 J. Zheng, Q. Wang, L. Shi, P. Peng, L. Shi and T. Li, *Angew. Chem., Int. Ed.*, 2021, **60**, 20858–20864.
118 Y. Zhao, Y. Zhao, Y. Ling, Z. Chen, X. Wu, X. Lu, Y. He, H. Wang and F. Dong, *Adv. Sci.*, 2025, **12**, e2416330.
119 N. Mahtal, O. Lenoir, C. Tinel, D. Anglicheau, P.-L. Tharaux, N. Mahtal, O. Lenoir, C. Tinel, D. Anglicheau and P.-L. Tharaux, *Nat. Rev. Nephrol.*, 2022, **18**, 643–662.
120 F. Ding, S. Zhang, Q. Chen, X. Xie, Z. Xi, Z. Ge, X. Zuo, X. Yang, I. Willner, C. Fan, Q. Li and Q. Xia, *Adv. Mater.*, 2024, **36**, e2310199.
121 J. V. Bonventre, V. S. Vaidya, R. Schmouder, P. Feig and F. Dieterle, *Nat. Biotechnol.*, 2010, **28**, 436–440.
122 Y. Sun, L. Mo, X. Hu, D. Yu, S. Xie, J. Li, Z. Zhao, X. Fang, M. Ye, L. Qiu, W. Tan and Y. Yang, *ACS Nano*, 2022, **16**, 21129–21138.
123 K. F. Wagenbauer, N. Pham, A. Gottschlich, B. Kick, V. Kozina, C. Frank, D. Trninic, P. Stömmer, R. Grünmeier, E. Carlini, C. A. Tsiverioti, S. Kobold, J. J. Funke, H. Dietz, K. F. Wagenbauer, N. Pham, A. Gottschlich, B. Kick, V. Kozina, C. Frank, D. Trninic, P. Stömmer, R. Grünmeier, E. Carlini, C. A. Tsiverioti, S. Kobold, J. J. Funke and H. Dietz, *Nat. Nanotechnol.*, 2023, **18**, 1319–1326.
124 P. S. Kwon, S. Ren, S.-J. Kwon, M. E. Kizer, L. Kuo, M. Xie, D. Zhu, F. Zhou, F. Zhang, D. Kim, K. Fraser, L. D. Kramer, N. C. Seeman, J. S. Dordick, R. J. Linhardt, J. Chao, X. Wang, P. S. Kwon, S. Ren, S.-J. Kwon, M. E. Kizer, L. Kuo, M. Xie, D. Zhu, F. Zhou, F. Zhang, D. Kim, K. Fraser, L. D. Kramer, N. C. Seeman, J. S. Dordick, R. J. Linhardt, J. Chao and X. Wang, *Nat. Chem.*, 2019, **12**, 26–35.
125 J. Spratt, J. M. Dias, C. Kolonelou, G. Kiriako, E. Engström, E. Petrova, C. Karampelias, I. Cervenka, N. Papanicolaou, A. Lentini, B. Reinius, O. Andersson, E. Ambrosetti, J. L. Ruas, A. I. Teixeira, J. Spratt, J. M. Dias, C. Kolonelou, G. Kiriako, E. Engström, E. Petrova, C. Karampelias, I. Cervenka, N. Papanicolaou, A. Lentini, B. Reinius, O. Andersson, E. Ambrosetti, J. L. Ruas and A. I. Teixeira, *Nat. Nanotechnol.*, 2023, **19**, 237–245.
126 M. You, G. Zhu, T. Chen, M. J. Donovan and W. Tan, *J. Am. Chem. Soc.*, 2015, **137**, 667–674.
127 R. Peng, X. Zheng, Y. Lyu, L. Xu, X. Zhang, G. Ke, Q. Liu, C. You, S. Huan and W. Tan, *J. Am. Chem. Soc.*, 2018, **140**, 9793–9796.
128 X. Chang, C. Zhang, C. Lv, Y. Sun, M. Zhang, Y. Zhao, L. Yang, D. Han and W. Tan, *J. Am. Chem. Soc.*, 2019, **141**, 12738–12743.
129 D. Wang, S. Li, Z. Zhao, X. Zhang and W. Tan, *Angew. Chem., Int. Ed.*, 2021, **60**, 15816–15820.
130 Y. Yang, J. Xu, Y. Sun, L. Mo, B. Liu, X. Pan, Z. Liu and W. Tan, *J. Am. Chem. Soc.*, 2021, **143**, 8391–8401.
131 Y. Zhao, F. Chen, Q. Li, L. Wang and C. Fan, *Chem. Rev.*, 2015, **115**, 12491–12545.
132 Y. Wang, X. Liu, Y. Zeng, S. K. Saka, W. Xie, I. Goldaracena, R. E. Kohman, P. Yin and G. M. Church, *Nucleic Acids Res.*, 2024, **52**, e71.
133 P. Sen, Z. Zhang, S. Sakib, J. Gu, W. Li, B. R. Adhikari, A. Motsenyat, J. L'Heureux-Hache, J. C. Ang, G. Panesar, B. J. Salena, D. Yamamura, M. S. Miller, Y. Li and L. Soleymani, *Angew. Chem., Int. Ed.*, 2024, **63**, e202400413.
134 Anusha, Z. Zhang, J. Li, H. Zuo and C. Mao, *J. Am. Chem. Soc.*, 2024, **146**, 25422–25425.
135 S. Liu, N. Hu, J. Hu, W. Li, S. Wu, X. Ma, Y. X. Huo and Y. Lu, *ACS Nano*, 2025, **19**, 25363–25384.
136 Y. Jia, S. Chen, Q. Wang and J. Li, *Nanoscale*, 2024, **16**, 2834–2846.
137 M. Herkt and T. Thum, *Mol. Ther.*, 2021, **29**, 521–539.
138 D. Wang, Q. Wang, Y. Wang, P. Chen, X. Lu, F. Jia, Y. Sun, T. Sun, L. Zhang, F. Che, J. He, L. Lian, G. Morano, M. Shen, M. Ren, S. S. Dong, J. J. Zhao, K. Zhang, D. Wang, Q. Wang, Y. Wang, P. Chen, X. Lu, F. Jia, Y. Sun, T. Sun, L. Zhang, F. Che, J. He, L. Lian, G. Morano, M. Shen, M. Ren, S. S. Dong, J. J. Zhao and K. Zhang, *Proc. Natl. Acad. Sci. U. S. A.*, 2022, **119**, e2113180119.
139 F. M. Anastassacos, Z. Zhao, Y. Zeng and W. M. Shih, *J. Am. Chem. Soc.*, 2020, **142**, 3311–3315.
140 T. R. Shepherd, R. R. Du, H. Huang, E.-C. Wamhoff, M. Bathe, T. R. Shepherd, R. R. Du, H. Huang, E.-C. Wamhoff and M. Bathe, *Sci. Rep.*, 2019, **9**, 6121.
141 R. Veneziano, T. J. Moyer, M. B. Stone, E.-C. Wamhoff, B. J. Read, S. Mukherjee, T. R. Shepherd, J. Das, W. R. Schief, D. J. Irvine, M. Bathe, R. Veneziano, T. J. Moyer, M. B. Stone, E.-C. Wamhoff, B. J. Read, S. Mukherjee, T. R. Shepherd, J. Das, W. R. Schief, D. J. Irvine and M. Bathe, *Nat. Nanotechnol.*, 2020, **15**, 716–723.
142 Y. C. Zeng, O. J. Young, C. M. Wintersinger, F. M. Anastassacos, J. I. MacDonald, G. Isinelli, M. O. Dellacherie, M. Sobral, H. Bai, A. R. Graveline, A. Vernet, M. Sanchez, K. Mulligan, Y. Choi, T. C. Ferrante, D. B. Keskin, G. G. Fell, D. Neuberg, C. J. Wu, D. J. Mooney, I. C. Kwon, J. H. Ryu, W. M. Shih, Y. C. Zeng, O. J. Young, C. M. Wintersinger, F. M. Anastassacos, J. I. MacDonald, G. Isinelli, M. O. Dellacherie, M. Sobral, H. Bai, A. R. Graveline, A. Vernet, M. Sanchez, K. Mulligan, Y. Choi, T. C. Ferrante, D. B. Keskin, G. G. Fell, D. Neuberg, C. J. Wu, D. J. Mooney, I. C. Kwon, J. H. Ryu and W. M. Shih, *Nat. Nanotechnol.*, 2024, **19**, 1055–1065.

